NASA CR 121024

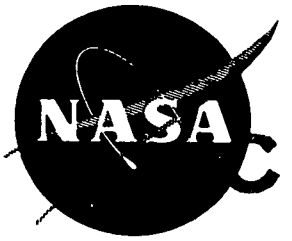

AN IMPROVED DESIGN METHOD AND EXPERIMENTAL PERFORMANCE OF TWO DIMENSIONAL CURVED WALL DIFFUSERS

BY

TAH-TEH YANG , W.G.HUDSON

AND ALI M. EL-NASHAR

CLEMSON UNIVERSITY

CLEMSON , SOUTH CAROLINA

PREPARED FOR

NATIONAL AERONAUTICAL AND SPACE ADMINISTRATION

NASA LEWIS RESEARCH CENTER

GRANT NGR 41-001-031

A. JUHASZ, PROJECT MANAGER

1. Report No.	2. Government Accession No.	3. Recipient's Catalog No.
CR-121024		

4. Title and Subtitle	5. Report Date
An Improved Design Method and Experimental Performance of Two Dimensional Curved Wall Diffusers	11/20/72
	6. Performing Organization Code

7. Author(s)	8. Performing Organization Report No.
Tah-teh Yang, W.G. Hudson, and Ali. M. El-Nashar	
	10. Work Unit No.

9. Performing Organization Name and Address	11. Contract or Grant No.
Mechanical Engineering Department Clemson University Clemson, South Carolina	NASA Grant NGR-41-001-031
	13. Type of Report and Period Covered
12. Sponsoring Agency Name and Address	Contractor Report
National Aeronautics and Space Administration Washington, D. C. 20546	14. Sponsoring Agency Code

15. Supplementary Notes

Project Manager, Albert J. Juhasz
Air Breathing Engines Division, NASA Lewis Research Center
Cleveland, Ohio

16. Abstract

A computer design program was developed to incorporate the suction slots in solving the potential flow equations with prescribed boundary conditions. Using the contour generated from this program, two Griffith diffusers were tested having area ratios AR = 3 and 4. The inlet Reynolds number ranged from 6×10^5 to 7×10^6. It was found that the slot suction required for meta-stable operation depends on the side-wall suction applied. Values of slot suction of 8% of the inlet flow rate was required for AR = 4 with meta-stable condition, provided that enough side-wall suction was applied. For AR = 3, the values of slot suction was about 25% lower than those required for AR = 4. For nearly all unseparated test runs, the effectiveness η was 100% and the exit flow was uniform. In addition to the Griffith diffusers, dump and cusp diffusers of comparable area ratios were built and tested. The results obtained from these diffusers were compared with those of the Griffith diffusers. Flow separation occurred in all test runs with the dump and cusp diffusers.

17. Key Words (Suggested by Author(s))	18. Distribution Statement
Contour wall diffuser Boundary layer control Diffuser performance Diffuser design	Unclassified - unlimited

19. Security Classif. (of this report)	20. Security Classif. (of this page)	21. No. of Pages	22. Price*
Unclassified	Unclassified	72	

* For sale by the National Technical Information Service, Springfield, Virginia 22151

FOREWORD

The research described herein, which was conducted by the Mechanical Engineering Department of Clemson University, was performed under NASA Grant NGR-41-001-031. Project Manager was Mr. Albert Juhasz of the Airbreathing Engines Division, NASA-Lewis Research Center.

TABLE OF CONTENTS

SUMMARY

This report presents the results of an investigation concerning the design and testing of two-dimensional subsonic short diffusers employing boundary layer control using suction slots. The main goal was to design and test a two-dimensional Griffith diffuser using an improved computer design program. This program incorporates the suction slots in the potential flow solution. The diffuser contour was arrived at by prescribing the potential flow velocity along the diffuser wall to have a region of constant high velocity at the inlet, a region of constant low velocity at the exit, and a region of concentrated deceleration connecting the inlet and exit regions. The suction slot was located at the deceleration zone to control flow separation within this region. Side-wall suction was applied through porous side walls in order to maintain two-dimensional flow. Two diffusers, with area ratios, AR, of 3 and 4, were tested. The inlet and diffuser lengths were 1.0 in (2.54 cm) and 6.2 in (15.7 cm) respectively. Slot suction rates around 8% of the inlet flow rate were required for the diffuser with AR = 4 under metastable operating conditions, provided enough side-wall suction was applied. Slot suction requirements for the diffuser with AR = 3 were about 25% lower when a constant side-wall suction of 15% of the inlet flow was applied. For stable operation the required slot suction ranged from 28 to 30 percent for the diffuser with AR = 3 and 30 to 34 percent for the diffuser with AR = 4. The values of the diffuser effectiveness η for the unseparated flow were very close to 100%. The flow emerging from the exit plane was uniform throughout most of the exit area. Good correlation was obtained between predicted and experimental values of wall pressure distribution and center line velocity distribution.

The secondary goal was to compare the performance of a dump (a dump diffuser is a sudden enlargement) and a cusp diffuser having variable area ratios between approximately 3 and 4 and having the same inlet and diffuser lengths as the Griffith diffuser. These diffusers were each fabricated with two different suction slot locations. For the dump diffuser, slots were provided at the inlet and exit corners; for the cusp diffuser the slots were located downstream of the cusp.

For the dump diffuser (AR = 3 and 4), the location of the suction slot proved to be critical regarding the diffuser effectiveness. With the suction slot located at the inlet corner, much higher values of effectiveness η were obtained than with the slot located at the exit corner. However, flow separation occurred in all the test runs.

For the cusp diffuser (AR = 2.7 and 3.7), it was not possible to achieve unseparated flow using the available suction capability. Accordingly, no standing vortices were observed. The flow behaved as a jet emerging from the diffuser inlet section and no pressure recovery was obtained.

SECTION I

INTRODUCTION

1.1 Background

Research on curved wall short two-dimensional diffusers employing boundary layer suction has been going on since 1969 at Clemson University [1][1]. The diffuser contour was arrived at by prescribing the potential flow velocity along the diffuser wall to have a region of constant high velocity at the inlet, a region of constant low velocity at the exit, and a region of concentrated deceleration connecting the inlet and exit regions. This contour is similar to that used on experimental high-lift laminar airfoils, originally suggested by A. A. Griffith [2] and is henceforth referred to as the Griffith diffuser. A suction slot was located at the deceleration zone in order to control flow separation of the retarded fluid. Suction through the diffuser side-walls was necessary in order to achieve two-dimensional flow. Test results indicated that a high diffuser effectiveness (98%) and a uniform exit velocity distribution were achieved. Suction rates several times higher than those predicted theoretically were necessary to achieve these results. It was pointed out in [1] that the incorporation of the suction slot in the potential flow solution was needed. This could result in a diffuser requiring a lower slot suction rate than the one previously designed.

A different approach towards designing an unseparated diffuser was taken by Ringleb [3]. He suggested a method of preventing separation by means of two standing vortices located near the boundaries of the flow

---

[1] Bracketed numbers refer to references in Section 8

passage. This was done by designing the contour of the flow passage in such a way as to allow the formation of two standing vortices with other flow control methods like boundary layer suction. A cusp provides the proper device for the standing vortices. Perkins and Hazen [4] have reported a successful attempt in using a short cusp diffuser.

1.2 Objectives

The primary objectives of this research effort described in this report were: (1) to re-examine experimentally the slot suction requirement in two-dimensional Griffith diffuser with diffuser contour determined from the improved design program. The improved design program treats the suction slot geometry as an integral part of the diffuser design. A slot suction requirement less than 10% was chosen as a limit of practical interest for an area ratio of 4 to 1. (2) to examine experimentally the interaction between the side-wall suction and the slot suction requirements.

The secondary objectives were: (1) to compare the performance, effectiveness and exit velocity distribution, of a dump diffuser (sudden enlargement) having the same area ratio and length to inlet width ratio as the Griffith diffuser at comparable suction rates. (2) to establish unseparated flow with standing vortices in a cusp diffuser having an area ratio comparable to the Griffith diffuser and compare its performance with that of the Griffith diffuser.

1.3 Scope

(1) Improve the existing design computer program which was used in the design of flow channels with prescribed boundary conditions (inlet, exit, and wall velocity distribution) to incorporate the suction slot in the

potential flow solution. Use the modified computer program to generate the contour of a Griffith diffuser.

(2) Use the existing analysis computer program [6] to analyze the flow field in the diffuser geometry generated from the improved design program.

(3) Use conformal mapping techniques described in Section 3.2.2 to arrive at the contour of a cusp diffuser having an area ratio of 4 to 1.

(4) Fabricate a Griffith, dump and cusp diffusers. Allowance was made in the design of the dump diffuser to have the suction slot location interchangeable between the inlet corner and the exit corner of the diffuser. Two suction slots were provided in the cusp diffuser, both downstream of the cusp. Only one suction slot was used at one time, the other was blocked.

(5) Carry out experimental tests to obtain the suction requirement for stable and meta-stable operations, effectiveness, wall velocity distribution, centerline velocity distribution and exit velocity distribution for each diffuser. Compare the measured and the analytically predicted velocity distributions. The range of the inlet velocity used was from 30 ft/sec (9 m/sec) to 260 ft/sec (79 m/sec).

SECTION II

SYMBOLS

A_i	cross sectional area at diffuser inlet
AR	area ratio, exit area to inlet area
A_{pq}	coefficient in equation A-6
A	constant in King's law
B_{pq}	coefficient in equation A-7
C, $\overline{C}$	complex constants in equation 28
F	complex potential, $\phi + i\psi$
i	used in complex numbers, defined as $\sqrt{-1}$
$\vec{i}$	unit vector along x-axis
$\vec{j}$	unit vector along y-axis
$\vec{k}$	unit vector along z-axis
$\vec{n}$	outward normal unit vector
N	number of segments, see equation A-6
P	static pressure at any location along the diffuser wall
P_o	stagnation pressure at end of air duct
P_i	static pressure at inlet section
P_c	static pressure at cusp line, see Figure 38
P_t	static pressure at vena contracta, see Figure 38
P_{atm}	atmospheric pressure
P_e	static pressure at exit section
p	any point either on the body surface or in the fluid
q	any point or segment on the body surface
r	distance between two points p and q, see Figure A-1
Re	Reynolds number, $\dfrac{(4A_i/\text{perimeter})\ U_i}{\text{fluid kinematic viscosity}}$

SP	cascade spacing
S	refers to body surface; also to area on body surface; also length along segment in two-dimensional or length along streamline
s	length along streamline
U	velocity
U_∞	free stream velocity
$\vec{U}_\infty$	free stream velocity vector
U_x	component of fluid velocity in x-direction
U_y	component of fluid velocity in y-direction
U_n	component of fluid velocity normal to body surface
U_t	component of fluid velocity tangential to body surface
U_i	average velocity in the diffuser's inlet plane
U_e	average velocity in the diffuser's exit plane
U_c	average velocity at cusp line
U_t	average throat velocity at vena contracta
U_1	wall velocity upstream of suction slot
U_2	wall velocity downstream of suction slot
U_{max}	maximum velocity
u_1	velocity inside the boundary layer upstream of suction slot
V	D.C. voltage of hot wire or hot film probe
V_o	D.C. voltage of hot wire or hot film probe at U = 0
V_{max}	maximum D.C. volt
W_{pq}	complex velocity at point p due to the segment q
X,Y,Z	cartezian coorindates
Z	complex coordinates of any point in the argand plane, z = x + iy
$Z_1^*, \overline{Z}_1^*$	complex constants in equations 30a and 30b
α	real number in equation 27

$\gamma, \overline{\gamma}$	complex constants in equation 28
θ, λ	angles
ζ	complex variable defined as $\xi + i\eta$
ξ, η	real and imaginary parts of ζ
ϕ	potential function
ψ	stream function
ρ	fluid density
η	diffuser effectiveness, defined by eq. (31)

SECTION III

ANALYSIS AND DESIGN

3.1 Two-Dimensional Griffith Diffuser

3.1.1 Design Concept

A wall velocity distribution was prescribed as shown in Figure 1.

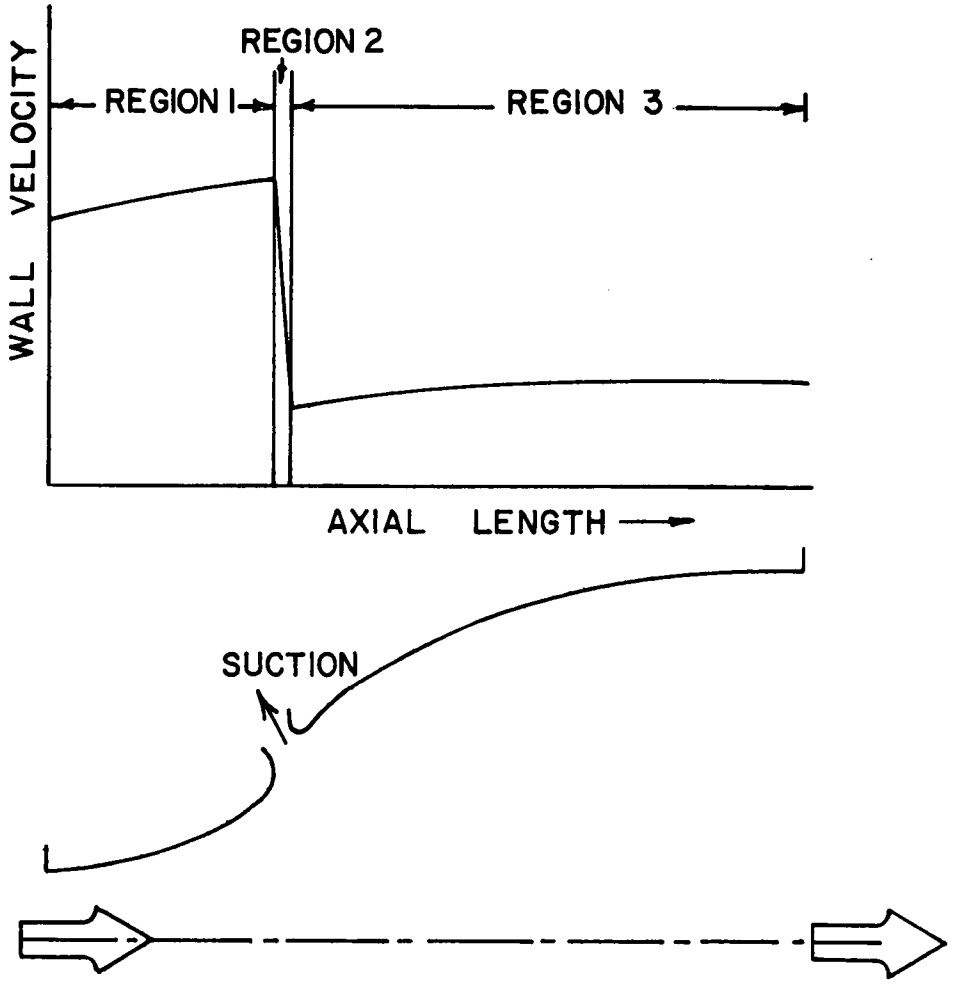

Figure 1. Velocity distribution along diffuser wall.

In region 1 and 3 an approximately constant wall velocities (with slight acceleration) were prescribed with all the adverse pressure gradient concentrated in a narrow region, region 2 in Figure 1. By confining the adverse pressure gradient to region 2, it may be possible to prevent wall separation in this region by applying boundary layer suction there through

a suction slot. This is aimed at removing the retarded fluid adjacent to the wall in this region.

G. I. Taylor provided a criterion for estimating the minimum suction requirement across a suction slot having a concentrated adverse pressure gradient. Taylor's criterion as reported in [7] is given by:

$$\frac{u_1}{U_1} = \sqrt{1.0 - \left(\frac{U_2}{U_1}\right)^2}$$

where U_1 and U_2 are the fluid velocities outside the boundary layers just upstream and downstream of the slot, u_1 is the velocity along the stagnation streamline just upstream of the slot, see Figure 2.

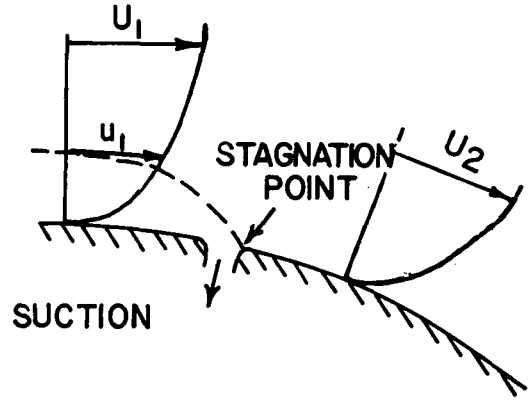

Figure 2. Flow over a suction slot.

In estimating the required suction rate, the boundary layer velocity distribution upstream of the slot is needed. Since the potential velocity upstream of the slot is prescribed to be nearly constant, the distribution may be approximated to be as that on a flat plate at constant free stream pressure. The geometry of the contoured wall can be obtained, assuming that the suction rate is sufficient to prevent flow

separation, by solving the inverse problem which is defined by prescribing the desired velocities at yet to be determined boundaries of the flow field.

3.1.2 Analysis

This section deals with the problem of determining the channel geometry for prescribed inlet, exit, and wall velocity distribution using two-dimensional imcompressible potential flow theory.

Following Stanitz [8] the analysis proceeds as follows: Consider two-dimensional irrotational motion in the physical XY plane, see Figures 3 and 4.

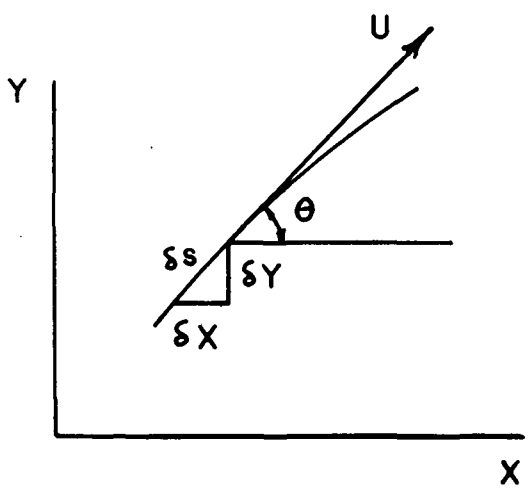

Figure 3. Direction of velocity at a point in XY-plane.

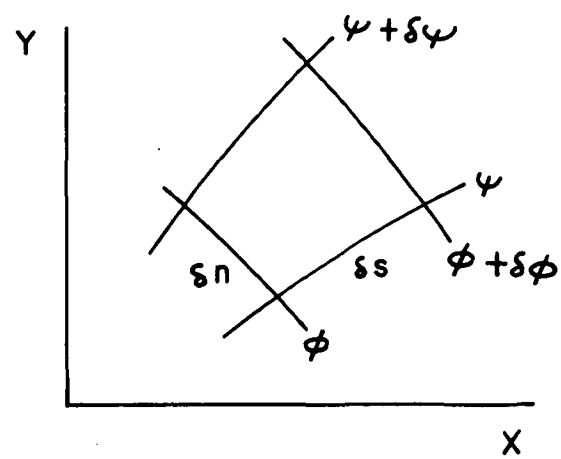

Figure 4. Streamlines and equipotential lines in XY-plane.

For an element of fluid of dimensions δs along the streamline and δn normal to it, the law of conservation of mass states that:

$$\frac{\partial}{\partial s}(\rho U \delta n) = 0 \tag{1}$$

For an incompressible flow:

$$\frac{\partial \ln U}{\partial s} + \frac{1}{\delta n}\frac{\partial(\delta n)}{\partial s} = 0 \tag{2}$$

From geometrical considerations:

$$\frac{1}{\delta n}\frac{\partial(\delta n)}{\partial s} = \frac{\partial \theta}{\partial n} \quad \text{and} \tag{3a}$$

$$\frac{1}{\delta s}\frac{\partial(\delta s)}{\partial n} = -\frac{\partial \theta}{\partial s} \tag{3b}$$

Using equations 3a and 3b into equation 2 yields:

$$\frac{\partial \ln U}{\partial s} + \frac{\partial \theta}{\partial n} = 0 \tag{4}$$

or

$$\frac{\partial \ln U}{\partial \phi}\frac{\partial \phi}{\partial s} + \frac{\partial \theta}{\partial \psi}\frac{\partial \psi}{\partial n} = 0 \tag{5}$$

But $d\psi = \rho U dn$ (6)

and $d\phi = U ds$ (7)

Using equations 5 and 6 into equation 5, we get:

$$\frac{1}{\rho}\frac{\partial \ln U}{\partial \phi} + \frac{\partial \theta}{\partial \psi} = 0 \tag{8}$$

Equation 8 is the equation of continuity for incompressible flow in the $\phi\psi$ - coordinate system.

The condition of irrotationality is:

$$\frac{\partial}{\partial n}(U\delta s) = 0 \qquad \text{(vorticity = 0)} \tag{9}$$

or

$$\frac{1}{\delta s}\frac{\partial \delta s}{\partial n} + \frac{\partial \ln U}{\partial n} = 0 \qquad (10)$$

Using equation 3b with equation 10 we get:

$$\frac{\partial \ln U}{\partial n} - \frac{\partial \theta}{\partial s} = 0$$

or

$$\frac{\partial \ln U}{\partial \psi}\frac{\partial \psi}{\partial n} - \frac{\partial \theta}{\partial \phi}\frac{\partial \phi}{\partial s} = 0 \qquad (11)$$

Introducing the relationships of equations 6 and 7 into equation 11 yields equation 12

$$\rho \frac{\partial \ln U}{\partial \psi} - \frac{\partial \theta}{\partial \phi} = 0 \qquad (12)$$

Equation 12 is the condition of irrotationality in the $\phi\psi$ - coordinate system.

From equations 8 and 12, equation 13 can be derived.

$$\frac{\partial^2 \ln U}{\partial \phi^2} + \frac{\partial^2 \ln U}{\partial \psi^2} = 0 \qquad (13)$$

Thus ln U satisfies the Laplace equation in the $\phi\psi$ - plane and with a given set of boundary conditions, ln U may be found over the entire ϕ-ψ region.

After equation 12 has been solved to obtain the distribution of ln U in the transformed $\phi\psi$ - plane (for the arbitrary specified variations in ln U with ϕ along the boundaries of constant ψ), the geometry of the diffuser in the physical xy - plane can be determined from the resulting distribution of flow direction θ. The flow direction θ can be determined from equation 8:

$$\theta = \int_{\psi} \rho \frac{\partial \ln U}{\partial \psi} d\phi \tag{14}$$

where ψ under the integral sign indicates that the integration is taken along a streamline (const. ψ) and where the constant of integration is selected to give a known value of θ at one value of ϕ along the stream line.

The distribution of the flow direction along an equipotential line (const. ϕ) is obtained from equation 8 which, after integration gives

$$\theta = \int_{\phi} \frac{1}{\rho} \left(\frac{\partial \ln U}{\partial \phi}\right) d\psi \tag{15}$$

where ϕ under the integral sign indicates that the integration is taken along an equipotential line (const. ϕ) and where the constant of integration is selected to give a known value of θ at one value of ψ along the equipotential line.

The variation in X and Y along a stream line is:

$$\left(\frac{\partial X}{\partial \phi}\right)_{\psi} = \left(\frac{\partial X}{\partial s} \frac{\partial s}{\partial \phi}\right)_{\psi} \tag{16}$$

Since from Figure 3, $\delta X = \delta s \cos \theta$ and $\delta Y = \delta s \sin \theta$ and since $\delta \phi = U \delta s$, then:

$$\frac{\partial X}{\partial \phi} = \frac{\cos \theta}{U} \tag{17}$$

and

$$X = \int_{\psi} \frac{\cos \theta}{U} d\phi \tag{18}$$

Similarly $$Y = \int_{\psi} \frac{\sin \theta}{U} d\phi \tag{19}$$

The variation in X and Y along an equipotential line are given by:

$$X = - \int_{\phi} \frac{\sin \theta}{\rho U} d\psi \tag{20}$$

and

$$Y = \int_{\phi} \frac{\cos\theta}{\rho U} d\psi \qquad (21)$$

The constants of integration are selected to give known values of X and Y at one value of ϕ along a streamline or at one value of ψ along an equipotential line.

3.1.3 Incorporation of Suction Slot in the Design

In the previous design of the Griffith diffuser which was reported in [1] no account was taken to the effect of slot suction on the channel geometry. In other words, it was assumed that suction at the walls does not affect the flow field or the geometry of the flow channel. This assumption may be justified for very small slot suction rates. The error thus introduced can no longer be negligible at the suction rates reported in [1]. An account of the way the slot suction was incorporates in the flow channel design is described below.

Instead of the simple geometry used before, the wall contour near the slot is now as shown in Figure 5.

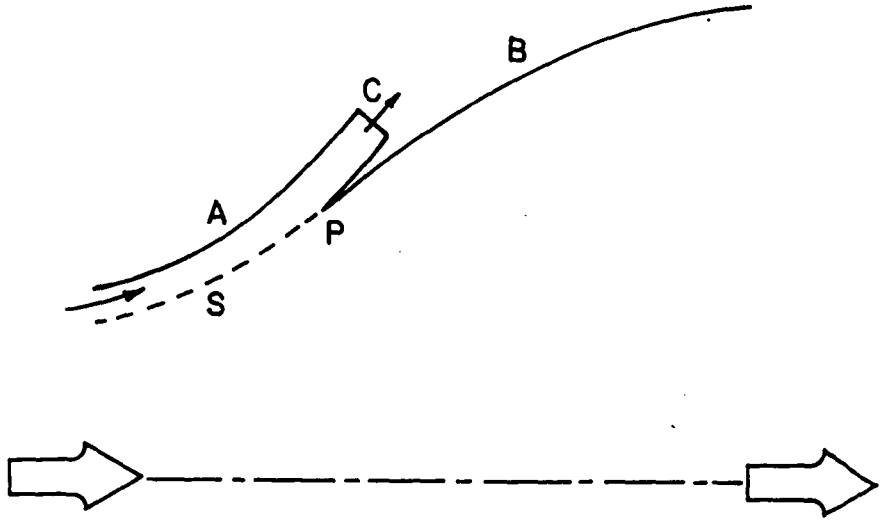

Figure 5. Diffuser geometry at slot location.

The suction flow was branched and leaving across the boundary C. As a consequence of this, the flow along the streamline s is brought to rest at a point p on the boundary just downstream of the slot.

Boundary line C was assumed to be an equipotential line (ϕ = const.) and the flow across it was assumed uniform and parallel. From equation 15, it can be seen that along line C, the following conditions must be satisfied:

$$\frac{\partial \ln U}{\partial \phi} = 0$$

On streamlines A and B any desired wall velocity distribution prescribed was as usual.

The existence of a stagnation point p on the channel wall introduced a singular point; U = o and hence ln U = $-\infty$. This presented a difficult situation for the computer to handle. To avoid this, Nelson [5] used a small portion of the potential flow solution of flow around a wedge was used into the finite difference mesh around the immediate vicinity of the wedge. In this way the stagnation point p could be isolated from the rest of the flow field and no infinite value encountered.

On the $\phi\psi$ - plane, the region around the wedge appears as in Figure 6 below.

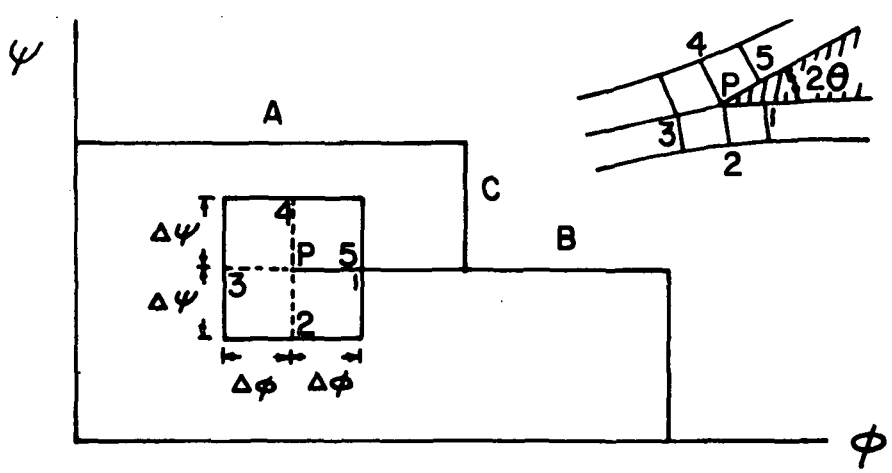

Figure 6. Wedge flow in $\phi\psi$-plane.

The velocities at points 2, 3, and 4 may be expressed from the wedge flow solution in terms of the velocity at point 1 as follows:

$$U_2 = \frac{\Delta\psi}{\Delta\phi}\left(\frac{\Delta\phi}{\Delta\psi}\right)\left(\frac{\pi-\theta}{\pi}\right) U_1 \tag{22}$$

$$U_3 = U_1 \tag{23}$$

$$U_4 = \frac{\Delta\psi}{\Delta\phi}\left(\frac{\Delta\phi}{\Delta\psi}\right)\frac{\pi-\theta}{\pi} U_1 \ . \tag{24}$$

Choosing $\Delta\phi = \Delta\psi$ leads to:

$$U_1 = U_2 = U_3 = U_4 = U_5 \tag{25}$$

3.1.4 Computer Design Program

Using the analysis outlined in 3.1.2 and 3.1.3, a digital computer program was utilized to solve equation 13 using the Gauss-Siedel numerical method. The program used numerical integration to obtain the coordinates of the various streamlines, including the outermost streamline which coincide with the channel wall geometry including the suction slot. This assumes, of course, a negligibie boundary layer thickness. The computer program was reported in [5] where an example was also presented to illustrate the details involved in preparing the input data for the design of an annular Griffith diffuser. A similar two-dimensional Griffith diffuser may be obtained merely by selecting an appropriate flag in the control card of the computer data deck.

3.1.5 Computer Analysis Program

After the diffuser geometry for a prescribed velocity distribution was obtained using the design program referred to in 3.1.4, the analysis program was used to calculate the velocities along the diffuser wall and in the flow field. This provided a means of checking the diffuser contour generated using the design program by comparing the velocity distributions

calculated using the analysis program with those prescribed in the design program. The analysis program was developed by Hess and Smith [5] and a subroutine was added to the original computer program to yield the velocities along the diffuser wall with suction rates ranging from 1% to 10% of the inlet flow in 1% increments. The program uses the surface - source - distribution method in solving channel flow problems using the cascade theory [6]. An outline of the theoretical analysis is given in Appendix A.

3.2 Cusp Diffuser

3.2.1 Background

This brief exploratory study was prompted by a theory proposed by Ringleb (Ref. 3) on what has become known as the cusp diffuser. It is suggested that the snow cornice sometimes observed on the ice side of a mountain ridge represents a natural flow-control device which causes the wind on the windward side of the ridge to expand smoothly over the ridge onto the ice side under the influence of a vortex situated in the cavity behind the cusp-like edge of the cornice, see Figure 7a. This is a natural flow separation-control device which may prove applicable in a diffuser, as in Figure 7b.

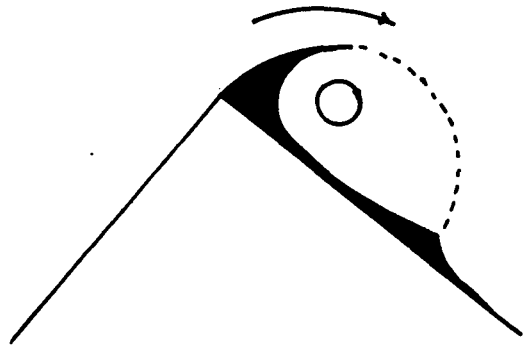

Figure 7a. Snow cornice flow.

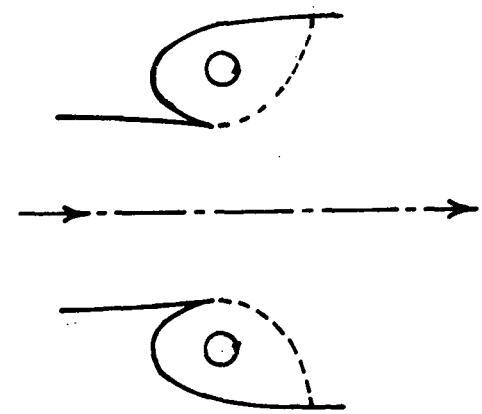

Figure 7b. Cusp diffuser.

The idea was used by Ringleb (Ref. 3) to build the Princeton University Cusp diffuser which proved, according to (Ref. 4), to be workable.

3.2.2 Contour Generation

The analysis makes use of conformal mapping techniques which transform the boundaries of the flow channel in the Z-plane into a simpler one in the ζ-plane. The flow field over the transformed boundaries can be readily known using a combination of sources, sinks and vortices. Transforming the known flow field back from the ζ-plane to the Z-plane yields the required flow field in the channel.

According to Riemann, for any simply connected area A in the Z-plane (physical plane) there exists a one-to-one conformation which maps this area onto the upper ζ-half plane. The transformation which maps the half plane into the area A is then given by the function:

$$Z = f(\zeta) \tag{26}$$

where

$$Z = x + iy; \quad \text{and } i = \sqrt{-1}$$

In transforming the ζ-half plane into a divergent contour with two cusps, two transformations were used, these are:

$$\text{(a) } Z^{*} = -\ln\left[(\zeta + i)^{\alpha} - i^{\alpha}\right] + \frac{i\alpha\pi}{2} \tag{27}$$

where α is a real number. This transforms the upper ζ-plane into a divergent duct with an area ratio $AR = \frac{\pi + \alpha\pi}{\alpha\pi} = 1 + \frac{1}{\alpha}$, see Figure 8.

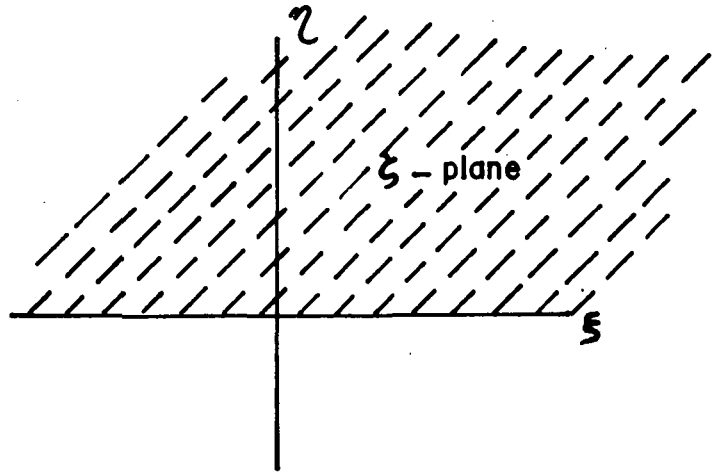

Figure 8a. ζ-plane.

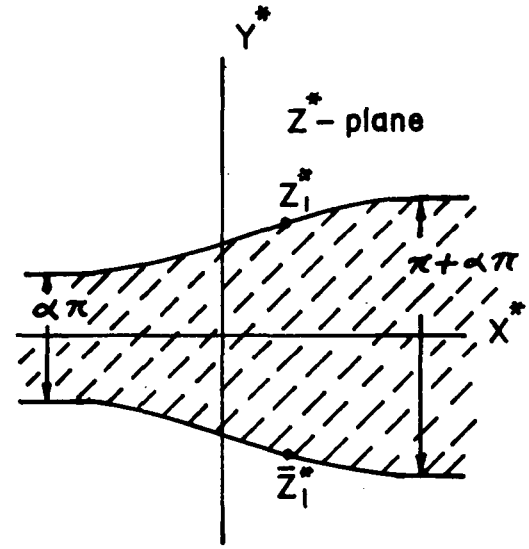

Figure 8b. Z^*-plane.

Figure 8. Mapping the upper ζ-plane onto a divergent channel using equation 27.

For an AR = 3 $\quad\quad \alpha = 1/2$

For an AR = 4 $\quad\quad \alpha = 1/3$

$$(b) \quad Z = Z^* + \frac{\gamma}{Z^* - C} + \frac{\bar{\gamma}}{Z^* - \bar{C}} \tag{28}$$

where γ, $\bar{\gamma}$, C, $\bar{C}$, are complex constants. $\bar{\gamma}$ and $\bar{C}$ are the conjugate complex values of γ and C respectively.

This transforms the shaded area in Figure 8b into the shaded area shown in Figure 9.

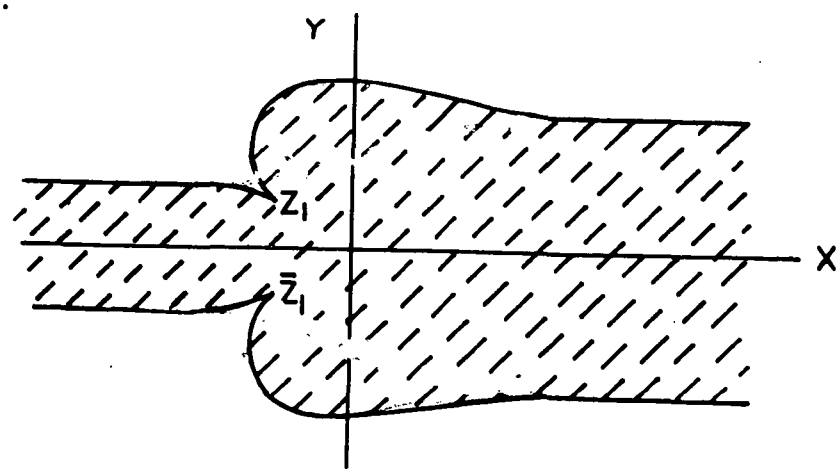

Figure 9. Mapping the shaded area in Figure 8b onto the Z-plane using equation 28.

The constants in equation 28 are calculated as follows:

(i) Select the cusp points Z_1^* and $\overline{Z}_1^*$ ($\overline{Z}_1^*$ is the conjugate value of Z_1^*) so that the cusps are slightly pointed toward the center of the flow passage.

(ii) Select the constants C anc $\overline{C}$ outside the duct in the Z^*-plane so that the cusps are joining the divergent channel smoothly.

(iii) From the condition that at the cusp points:

$$\frac{dZ}{dZ^*} = 0 \tag{29}$$

we get:

$$1 - \frac{\gamma}{(Z_1^* - C)^2} - \frac{\overline{\gamma}}{(Z_1^* - \overline{C})^2} = 0 \tag{30a}$$

and

$$1 - \frac{\gamma}{(\overline{Z}_1^* - C)^2} - \frac{\overline{\gamma}}{(\overline{Z}_1^* - \overline{C})^2} = 0 \tag{30b}$$

Equations 30a and 30b can be solved simultaneously and the constants γ and $\overline{\gamma}$ determined. With the constants in equation 28 now known, it is possible to generate the contour of the cusp diffuser.

SECTION IV

APPARATUS AND INSTRUMENTATION

4.1 Test Facility

A schematic of the test facility is shown in Figure 10. A pictorial view is shown in Figure 11. It consists of a 10,000 CFM (4.72 m^3/sec) fan powered by a 30 HP motor, delivering air to a 20 ft. (6.1 m) long circular air duct having a diameter of 20 inches (50.80 cm). A shutter type damper at the fan inlet was used to regulate the flow rate. A 24-inch (61.0 cm) diameter circular plate was located at the downstream end of the duct. This was used as a means of connecting the diffuser to the duct.

In order to achieve a uniform inlet air velocity to the diffusers, a flow-straightening section and a set of 4 fine screens were installed in the duct. The flow-straightening section was 5 ft. (1.52 m) long containing tubes of 1.25 inches (3.18 cm) diameter. The set of fine screens had mesh sizes of 20, 40, 50, and 100 per inch and were installed in the sequence of increasing mesh number in the flow direction.

Suction was applied through the slots in the diffuser walls and through the side walls. This was necessary both to control separation and to achieve a two-dimensional flow through the diffuser. The sub-atmospheric suction pressure was provided by two positive displacement blowers each rated at 300 CFM (0.142 m^3/sec) at 5 inches of Hg (12.7 cm Hg) vacuum. The two blowers were powered by a 15 HP motor. Suction flow rate was controlled using a bypass line and regulating gate values.

4.2 Griffith Diffuser

The computer design program [5] provided the contour of the diffuser (AR = 4). Figure 12 shows the coordinate and the contour resulting from

the design program. A computer plot of the diffuser contour is shown in Figure 13. Figure 14 shows the wall velocity distribution prescribed to the design program with 5% of the through flow as the design suction rate for the suction slots, and for AR = 4.

The diffuser was fabricated from aluminum stock to tolerances within one-thousandth of an inch (.0025 cm). The side walls were fabricated from a sintered porous stainless steel plate. A pictorial view of the diffuser, attached to a circular plate, is shown in Figure 15. The circular plate provided a means of connecting the diffuser to the air duct.

4.3 Dump Diffuser

The dump diffusers used were simply sudden enlargements with area ratios of 3 and 4. Suction slots were provided either at the inlet or exit corner; Figure 16 shows two revisions of a dump diffuser with the slots located at either the exit corners or at the inlet corners.

4.4 Cusp Diffuser

Using the method outlined in 3.2.2, the contour was generated using the transformation equation 28. The constants C and γ used are:

$$c = 0.150 + 1.050i, \qquad \gamma = -0.134 + 0.208i$$

Figure 17 shows the resulting coordinates and contour. Two suctions slots were provided on each wall on the downstream side fo the cusp. This would help to stability two trapped vortices [3]. Side-wall suction was also provided. The diffuser had the same inlet and diffuser length as both the Griffith and dump diffusers, 1 inch (2.54 cm) for inlet

length and 6.2 inch (15.7 cm) for diffuser length). Using these dimensions it was not possible to design a cusp diffuser with an area ratio of 4; the resulting diffuser had an area ratio of 3.7. This approximated the desired area ratio of 4 and may be set as 2.7 to approximate 3 by moving the two halves of the diffuser walls relative to each other in a direction normal to the air flow. Figure 18 shows a pictorial view of the two contoured walls of the cusp diffuser.

4.5 Instrumentation and Measurements

The stagnation pressure at the end of the air duct and the static pressure at the diffuser inlet were measured using a Meriam-type-Micro micromanometer with a resolution of 0.001 inch (0.0025 cm) of water. Using the Bernoulli equation and the difference of the above measured pressure readings the inlet velocity was determined.

The wall pressure distribution was measured using a differential pressure transducer with a range 0 - 1.0 psid (0 - 0.69 N/cm^2) having an error of 0.5% of the full scale, along with a rapid scanning mechanism with a capacity of 48 channels. The number of wall pressure taps on each wall was as follows:

Griffith Diffuser	17
Dump Diffuser	18
Cusp Diffuser	17

The output voltage from the pressure transducer was measured using a Digitec 269 Multimeter digital voltmeter and automatically recorded on paper tape for subsequent analysis.

The exit and center line velocity distribution were measured using hot wire and hot film probes in conjunction with a constant temperature anemometer. The use of either probe depended mainly on availability.

The D.C. voltage output of the probe was displayed by a multi-range Disa-type 55 D30 digital voltmeter. The probe was positioned using a traversing mechanism which had a resolution of 0.001 inch (0.0025 cm) in each of the three perpendicular directions.

The exit velocity distribution was obtained by making side-wall to side-wall velocity traverses along seven rows in the exit plane, see Figure 19. Along each row 19 measurements were taken which makes the total number of exit velocity measurements to be 133. Exit velocity distributions for the area ratio of 3 and 4 were obtained. In addition to the exit velocity distributions, axial velocity measurements were taken at several positions along the diffuser axis in the flow direction. The main through flow at the diffuser inlet section was estimated from the measured pressure difference between the inlet section and the plenum chamber at the end of the air duct. The exit velocity distribution and the flow through the suction passages measured by using venturi meters provided a check on the value of the inlet flow estimated by using the inlet area and the inlet velocity measurement mentioned earlier.

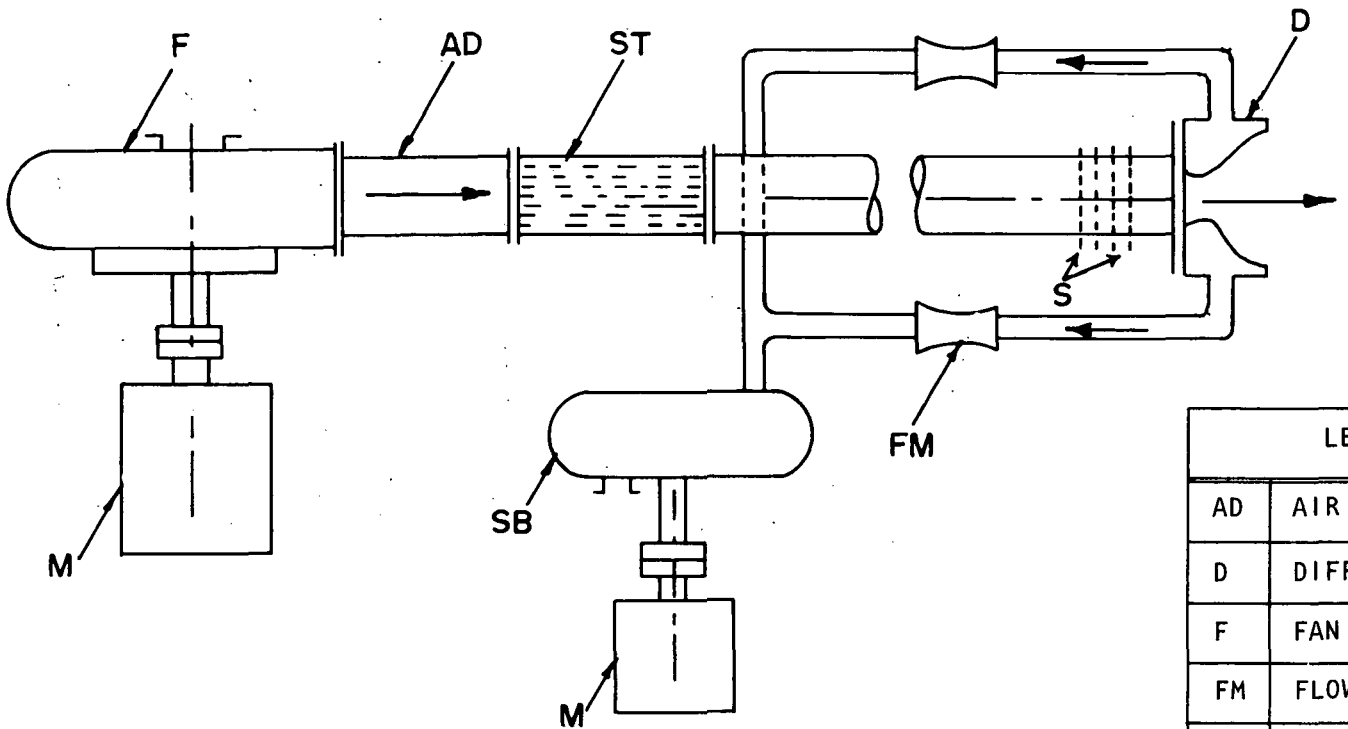

LEGEND	
AD	AIR DUCT
D	DIFFUSER
F	FAN
FM	FLOW METER
M	MOTOR
S	SCREENS
SB	SUCTION BLOWER
ST	STRAIGHTENER

Figure 10. Schematic of test facility

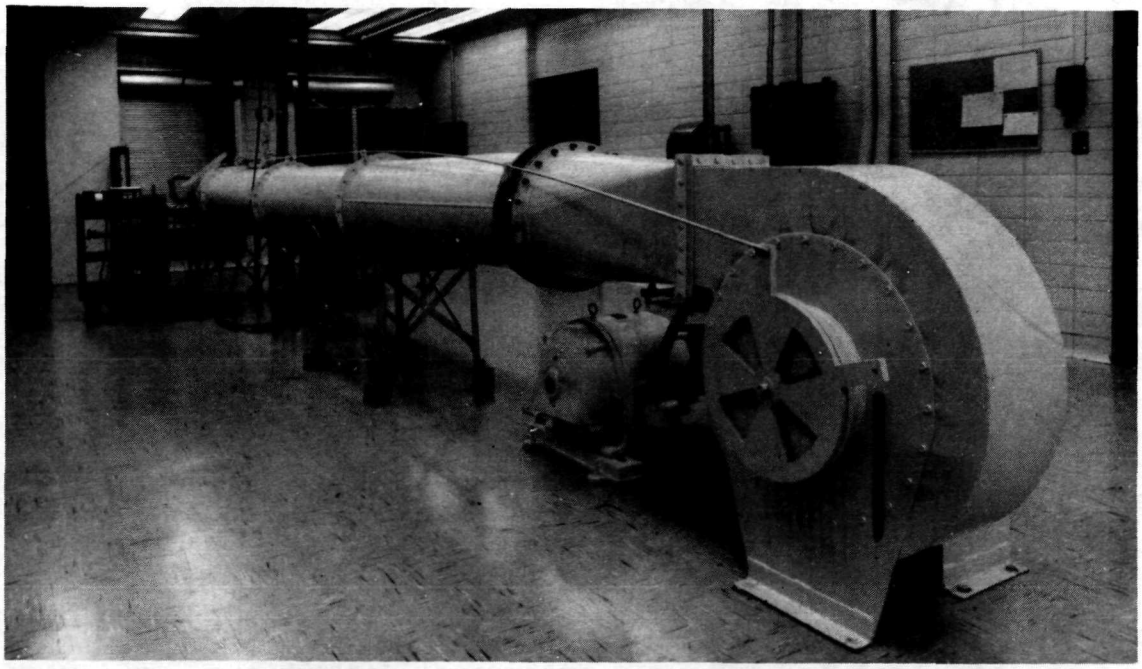

Figure 11. Pictorial view of test facility looking downstream

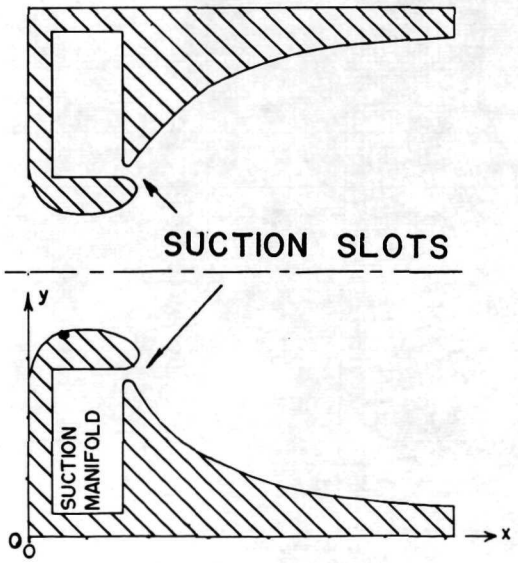

Figure 12a. Contour of Griffith diffuser

x		y		x		y	
in	cm	in	cm	in	cm	in	cm
0.00	0.00	2.60	6.60	3.20	8.13	1.28	3.25
0.10	0.25	3.17	8.05	3.60	9.14	1.11	2.82
0.20	0.51	3.28	8.33	4.00	10.16	0.97	2.46
0.40	1.02	3.40	8.64	4.40	11.18	0.85	2.16
0.60	1.52	3.46	8.79	4.80	12.19	0.76	1.93
0.90	2.29	3.50	8.89	5.20	13.21	0.69	1.75
1.20	3.05	3.48	8.84	5.60	14.22	0.63	1.60
1.60	4.06	3.36	8.53	6.00	15.24	0.582	1.48
2.00	5.08	2.19	5.56	6.40	16.26	0.55	1.40
2.40	6.10	1.78	4.52	6.80	14.73	0.52	1.32
2.80	7.11	1.49	3.78	7.19	18.26	0.50	1.27

Figure 12b. Coordinates of Griffith diffuser

Figure 12. Coordinates and contour of Griffith diffuser

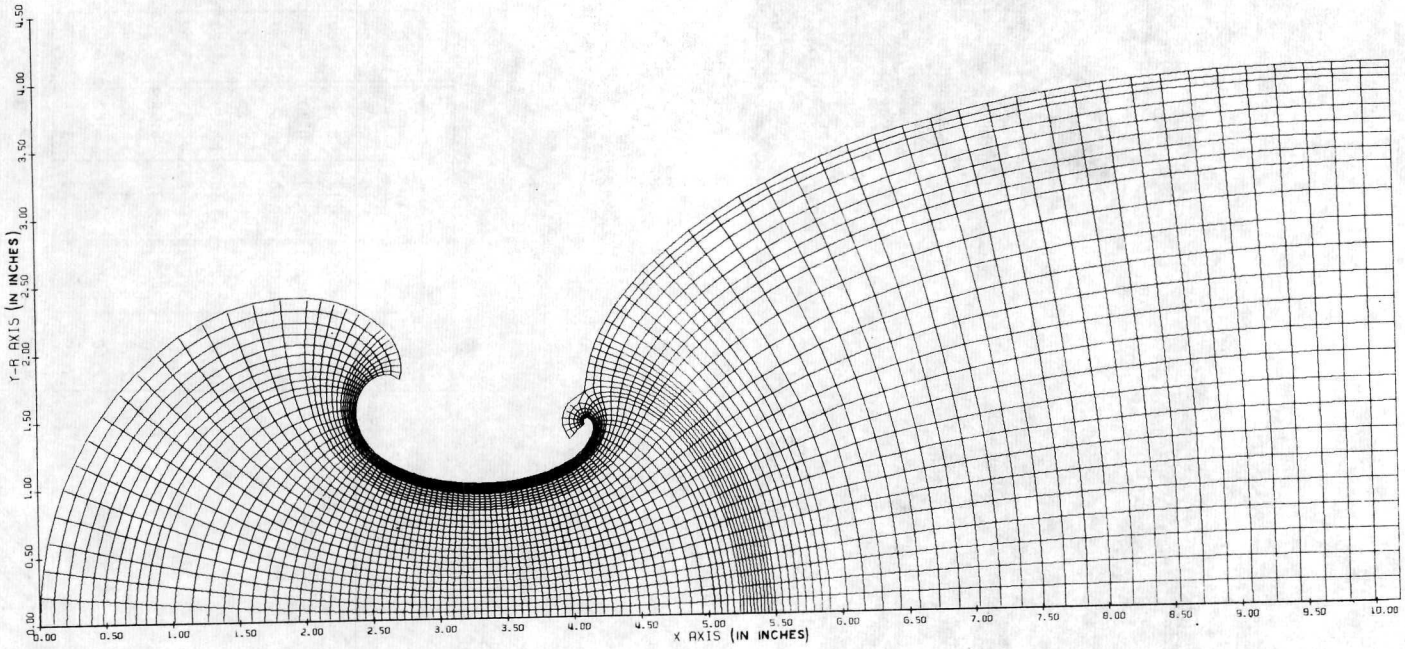

Figure 13. Computer plot for Griffith diffuser contour showing streamlines and equipotential lines.

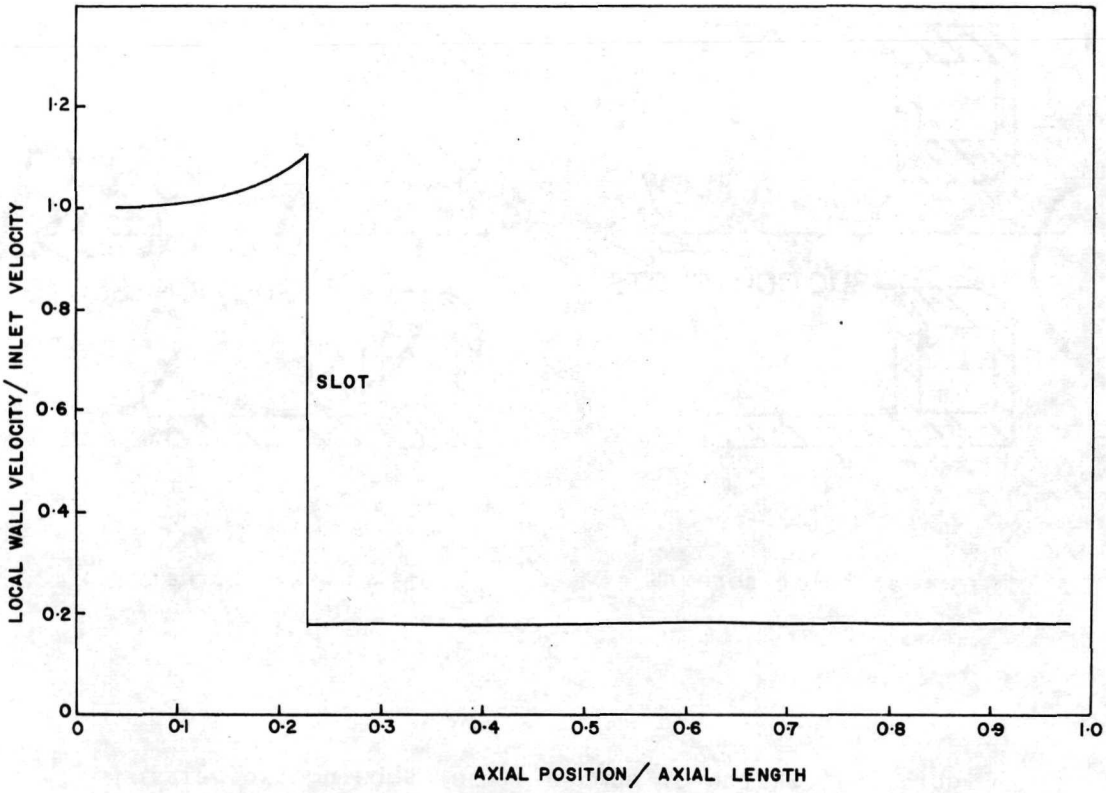

Figure 14. Wall velocity distribution prescribed to the computer design program for Griffith diffuser; AR $\doteq$ 4

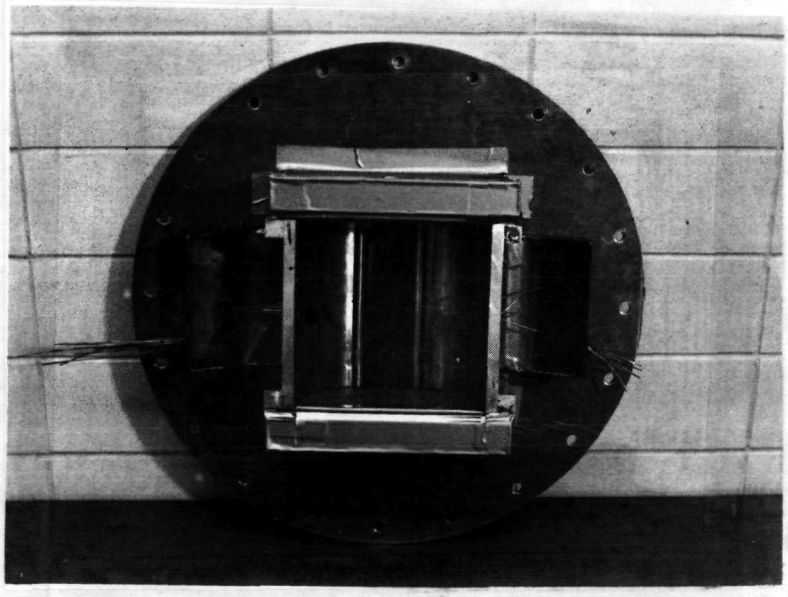

Figure 15. Griffith diffuser attached to circular plate

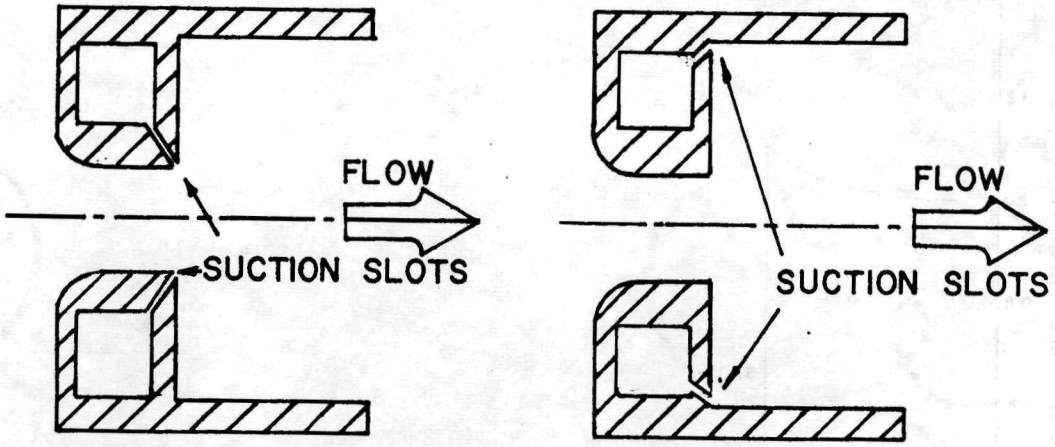

Slots at inlet corners

Slots at exit corners

Figure 16. Sketch of dump diffuser showing two versions of suction slot locations

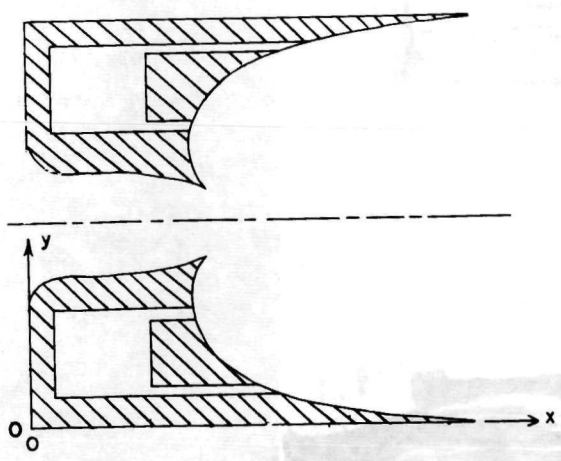

x		y		x		y	
in	cm	in	cm	in	cm	in	cm
0	0	2.18	5.54	2.8	7.11	2.77	7.04
0.2	0.51	2.44	6.20	2.8	7.11	2.65	6.73
0.4	1.02	2.53	6.43	2.8	7.11	2.64	6.71
0.7	1.78	2.57	6.53	2.9	7.37	2.80	7.11
1.2	3.05	2.57	6.53	2.9	7.37	1:49	3.78
1.4	3.56	2.58	6.55	3.2	8.13	1.15	2.92
1.6	4.06	2.59	6.58	4.0	10.16	0.62	1.57
1.8	4.57	2.59	6.58	4.8	12.19	0.40	1.02
2.0	5.08	2.61	6.63	5.6	14.22	0.27	0.68
2.4	6.10	2.67	6.78	6.6	16.76	0.12	0.30
2.7	6.86	2.73	6.93	7.4	18.80	0.00	0.00
2.7	6.86	2.10	5.33				

Figure 17a. Contour of cusp diffuser

Figure 17b. Coordinates of cusp diffuser

Figure 17. Coordinates and contour of cusp diffuser

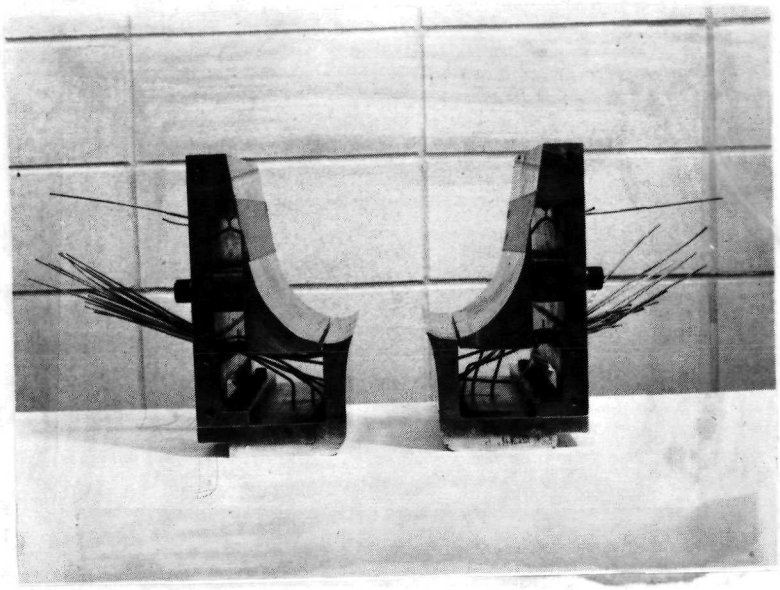

Figure 18. Pictorial view of cusp diffuser

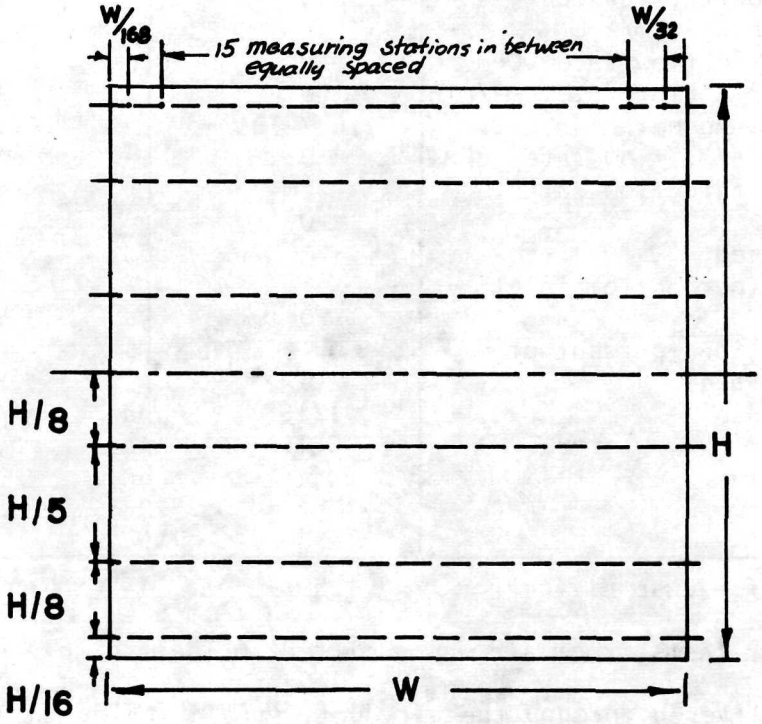

Figure 19. Exit velocity traverse locations

SECTION V

TEST CONDITIONS, PROCEDURE AND DATA REDUCTION

5.1 Test Conditions

To achieve the outlined project objectives, a comprehensive experimental investigation was carried out for the Griffith diffuser. To a lesser degree, experiments were conducted on both the dump and the cusp diffusers.

Table 1 gives a summary of the range of test parameters used in the tests for all three types of diffusers.

Table 1: Range of Test Parameters

Test Parameter	Range		
	From		To
Inlet air velocity, ft/sec	30		260
Inlet air velocity, m/sec	9		79
Inlet volumetric flow rate, CFM	0		2500
Inlet volumetric flot rate, m^3/min	0		70
Inlet Reynolds number	6×10^5		7×10^6
Suction volumetric flow rate, CFM	0		600
Suction volumetric flow rate, m^3/min	0		17
Area ratios used	3*	and	4*
Slot suction (percent of inlet flow rate)	0		50
Side-wall suction (percent of inlet flow rate)	0		35
Slot width, inch	1/16	and	1/4
Slot width, cm	0.16	and	0.64
Slot length, in		8	
Slot length, cm		20.3	

*2.7 and 3.7 for cusp diffuser

For all diffuser tests, room air was admitted to the fan through the shutters and delivered through the air duct, straightening tubes and screens to the diffuser and discharged back into the room.

5.2 Test Procedure and Data Reduction

Each test was conducted to obtain the following informations in the sequence indicated:

(a) Find the minimum slot suction requirements for both meta-stable and stable operating conditions for different inlet air velocities and for a constant side wall suction rate.

(b) Find the value of the diffuser effectiveness η for different values of inlet air velocity for the case of attached flow.

(c) Find the diffuser wall velocity distribution by taking wall static pressure readings using the pressure transducer.

(d) Find the exit velocity distribution by making horizontal traverses at the exit plane by taking exit velocity measurements using the hot wire or hot film probe.

(e) Find diffuser axial center line velocity distribution by making an axial traverse.

The following procedure and relationships for data reduction were used. In order to obtain the minimum slot suction requirement for meta-stable operating condition for a particular inlet air velocity the suction rate was first increased to achieve attached flow. The suction rate was then gradually reduced until the flow pattern in the diffuser changed from the attached to the separated condition as indicated by tufts on the exit walls. At this point the suction rate was slightly increased to restore the flow to the attached condition and all the necessary measurements were taken at the diffuser exit. Any interference

with the boundary layer at the slot or upstream of the slot would cause the flow to be separated. Therefore no probe was inserted in this region.

The minimum slot suction requirement for the stable operating condition for a particular inlet air velocity was obtained by increasing the slot suction beyond that required for minimum meta-stable operating condition. With the attached flow condition now achieved, a test for stability was performed. This was done by physically disturbing the boundary layer at, and upstream, of the slot; for example by touching these areas by hand. This would cause an immediate boundary layer separation. If slot suction was enough to maintain stable operation, the flow would be restored to its previous attached condition once the disturbance was removed. Otherwise, the suction had to be increased and the test repeated until the condition of stability obtained.

The diffuser effectiveness was estimated from three independent pressure measurements made using the micromanometer: (1) the static pressure at the diffuser inlet, P_i; (2) the static pressure at the end of the air duct, P_o; (3) the static pressure at the diffuser exit, P_e. From these three pressure measurements and from the previously measured total suction requirement, the diffuser effectiveness η was calculated from:

$$\eta = \frac{(P_e - P_i)}{(P_o - P_i)\left[1.0 - \left(\frac{1.0 - \frac{\%\ \text{total suction}}{100}}{AR}\right)^2\right]} \qquad 31$$

The derivation of this relation is given in Appendix B.

The diffuser wall velocity distribution was estimated from the wall static pressure measurements provided by the differential pressure

transducer. The transducer provided values for the pressure difference between the stagnation pressure P_o at the end of the air duct and the pressure P at any particular location along the diffuser wall. From these measurements the ratio of the wall velocity U at any particular location to the wall velocity U_i at the inlet section was calculated by:

$$\frac{U}{U_i} = \sqrt{\frac{P_o - P}{P_o - P_i}}$$

Both the exit velocity distribution and the center line velocity distribution were estimated from either constant temperature hot wire or hot film probe measurements using King's law:

$$V^2 = V_o^2 + A\sqrt{U}, \qquad V \text{ is the D.C. voltage}$$

at any velocity U and V_o is the D.C. voltage at U = 0 and A is a constant. Several probes were calibrated against pitot-static tubes and the results justified the use of King's law. The ratio of the velocity at any location U to the maximum velocity U_{max} is given by:

$$\frac{U}{U_{max}} = \left(\frac{V^2 - V_o^2}{V_{max}^2 - V_o^2}\right)^2$$

where V_{max} is the D.C. voltage corresponds to U_{max}.

SECTION VI

DISCUSSION OF RESULTS

6.1 Griffith Diffuser

Figure 20 shows the minimum slot suction requirement for constant values of side-wall suction rate expressed in percent of volumetric inlet flow rate for the diffuser with area ratio, AR = 4, and slot width = 1/8 inch (0.32 cm). The value of minimum slot suction requirement for the metastable condition and for a particular inlet velocity depends on the percent side-wall suction applied. At an inlet velocity of 100 ft/sec (30.5 m/sec) the slot suction requirement drops by 50% by increasing the side-wall suction from 10% to 25%. The amount of reduction in slot suction decreases as the side-wall suction continues to increase. This becomes obvious if one examines the effect of increasing the side-wall suction

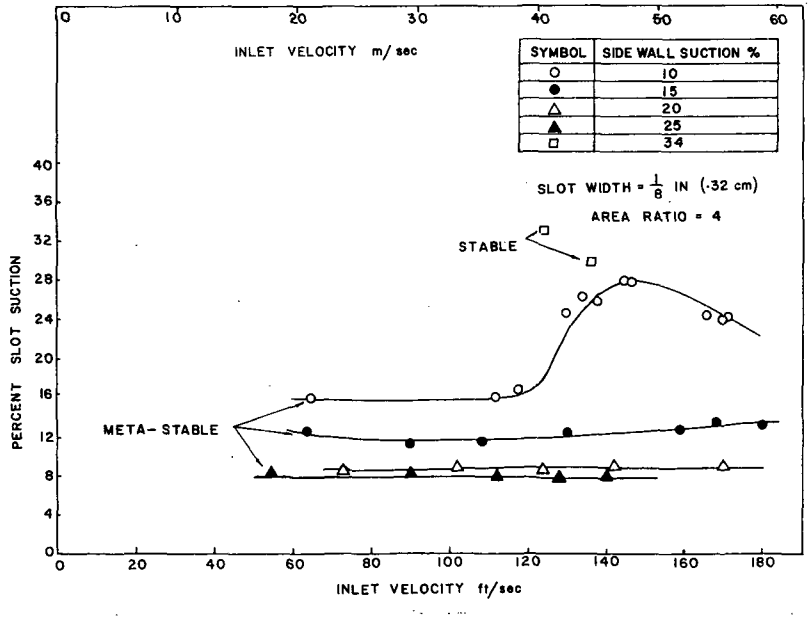

Figure 20. Percent-Slot suction versus inlet velocity for Griffith diffuser; AR = 4; slot width = 1/8 in (0.32cm)

from 10% to 25% in steps of 5% for an inlet velocity of 100 ft/sec (30.5 m/sec). An increase of side-wall suction of from 10% to 15% causes a reduction in slot suction of 28%, while an increase of from 20% to 25% causes a reduction of only 5%. Due to limitations in suction capability, it was not possible to achieve stable operating condition for more than few cases. Figure 21 shows the minimum meta-stable slot suction requirements for the same area ratio, AR = 4, but with a slot width double that of Figure 20; 1/4 inch (0.64 cm). The same trend is observed, i.e. an increase in the percent side-wall suction reduces the minimum slot suction requirement to achieve meta-stable operating condition. In this case; slot width = 1/4 inch (0.64 cm); the values of the slot suction requirements seem to be higher than the values for the case where slot width = 1/8 inch (0.35 cm).

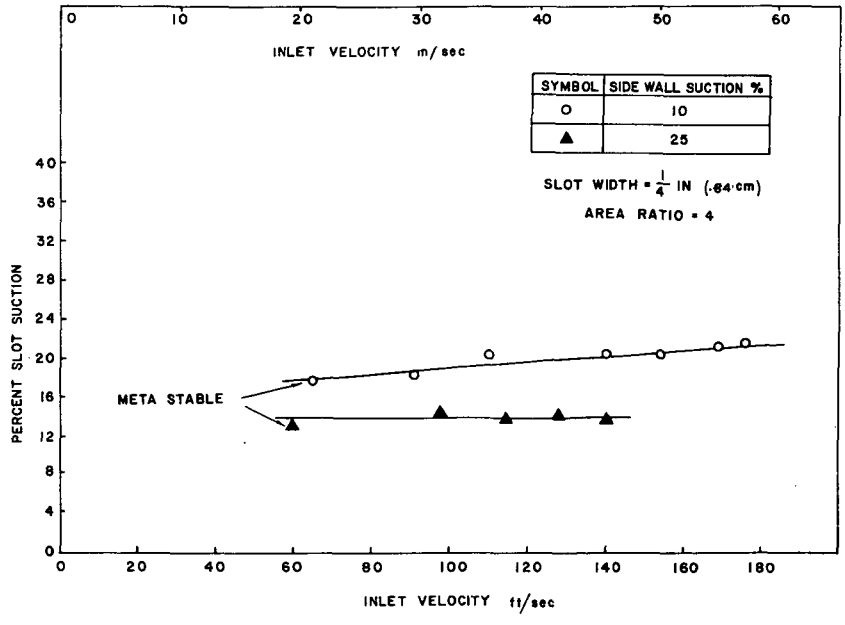

Figure 21. Percent slot suction versus inlet velocity for Griffith diffuser; AR = 4; slot width = 1/4 in (0.64 cm)

For a side-wall suction of 25%, the slot suction requirement is about 14% for the wide slot while for the narrow slot it is only about 8%.

The effect of area ratio on the minimum suction requirement is shown in Figure 22 for two area ratios, AR = 3, 4, and for a 15% side-wall suction. As would be expected, the diffuser with the smaller area ratio; AR = 3; requires a smaller percent slot suction to achieve meta-stability than would the larger one with AR = 4. The reduction in meta-stable slot suction requirement for the small area ratio, AR = 3, is about 25%, for the same side-wall suction of 15%. Using Taylor's criterion, and the 1/7th power law to approximate the velocity distribution in the boundary layer, the percent reduction in slot suction for AR = 3 was estimated to be 18%.

For stable flow, the required suction rate ranged from 28 to 30 percent for the diffuser with AR = 3.

It is apparent that slot suction percentages within a practical range can be achieved at the expense of higher side-wall suction percentages. It is believed that high side-wall suction was necessary because the boundary layer thickness at the corner between the diffuser walls and the side walls was several times thicker than elsewhere.

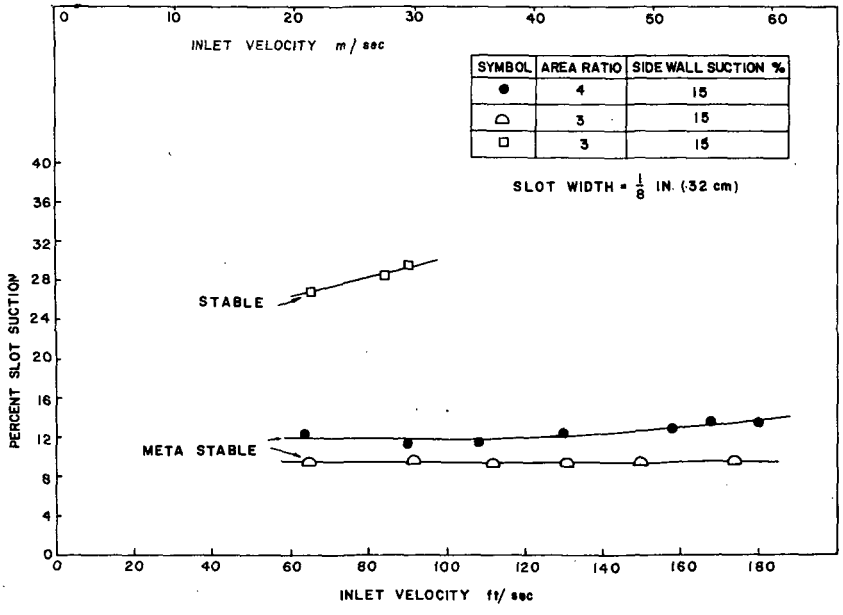

Figure 22. Percent slot suction versus inlet velocity for Griffith diffuser; AR = 3 and 4; slot width = 1/8 in (0.32 cm)

Referring to Figure 20.13 page 576 of Schlichting's Boundary Layer Theory [9] one notices that the boundary layer thickness at the corner of a noncircular duct is several times thicker than along the flat surfaces. Accordingly, it was more likely that separation would start at the junction of the diffuser walls and the side walls. Although no attempt was made at applying more suction along all the corners, several trials were made aiming at reducing the side-wall suction requirement by drilling several small holes in the sintered porous side plates in the region where the slots meet the side plates. This would apply more suction to the junction between the slot and the side walls and reduce the chance of separation in this region. No appreciable reduction in required side-wall suction was achieved.

The diffuser effectiveness, η, of 14 test runs are shown in Figure 23 over an inlet air velocity range of 50 ft/sec (15.2 m/sec) to 180 ft/sec (54.9 m/sec) for both area ratios of 3 and 4 and for slot widths of

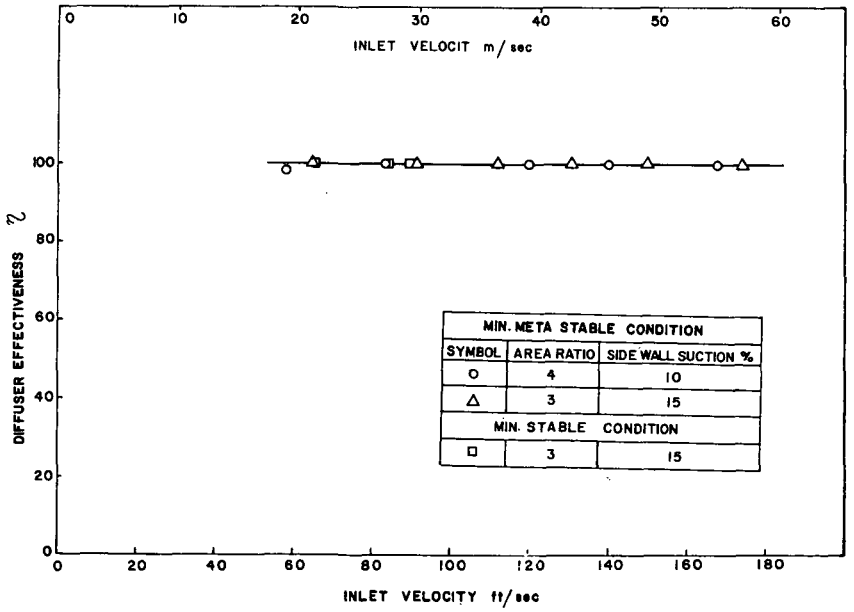

Figure 23. Effectiveness η versus inlet velocity for Griffith diffuser; AR = 4.

1/8 inch (0.32 cm) and 1/4 inch (0.64 cm). A 100% pressure recovery is achieved using the suction percentages shown in Figures 20 and 21. Similar values of η were reported in [1]. In Figure 24 the diffuser effectiveness is shown for varying values of slot suction with constant side-wall suction for stable and meta-stable operations. At values of slot suction higher than the minimum required in each case, the effectiveness has a value of 100%. As the value of slot suction is reduced below the minimum, the effectiveness drops sharply from 100% to about 15%. This is the value of the effectiveness with separated flow.

The wall velocity distributions as calculated from the diffuser wall static pressure measurements are shown in Figures 25 and 26 for

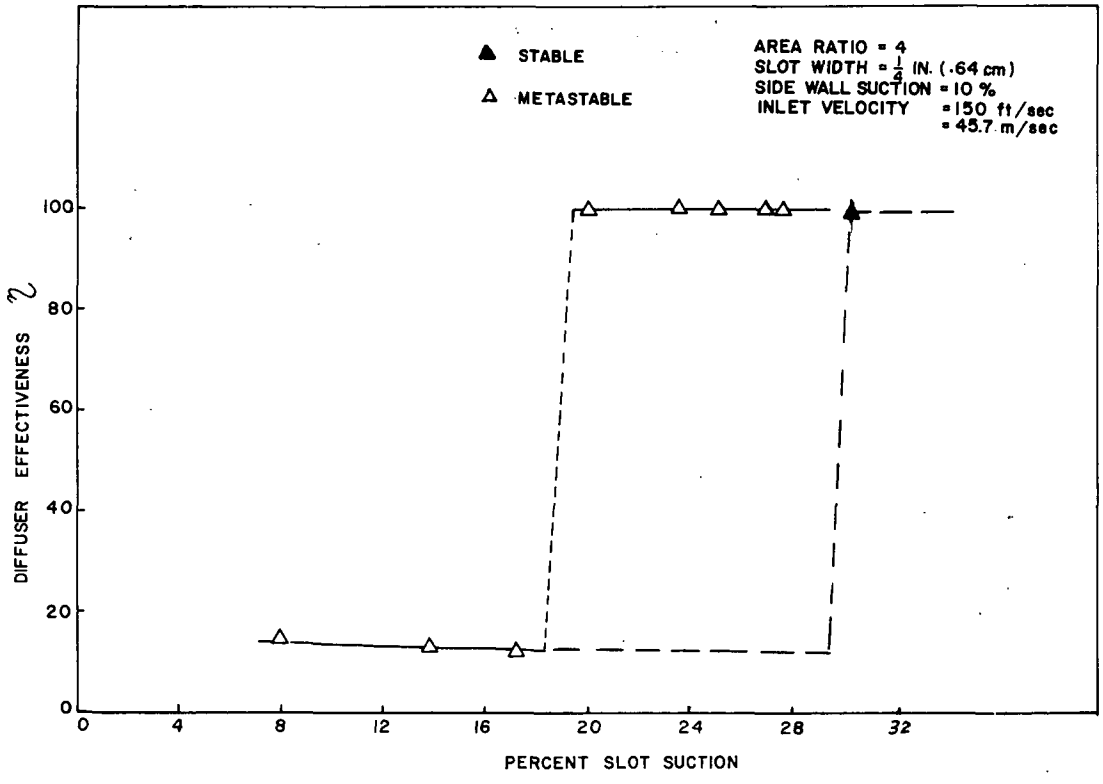

Figure 24. Effectiveness η versus percent slot suction for Griffith diffuser; AR = 4.

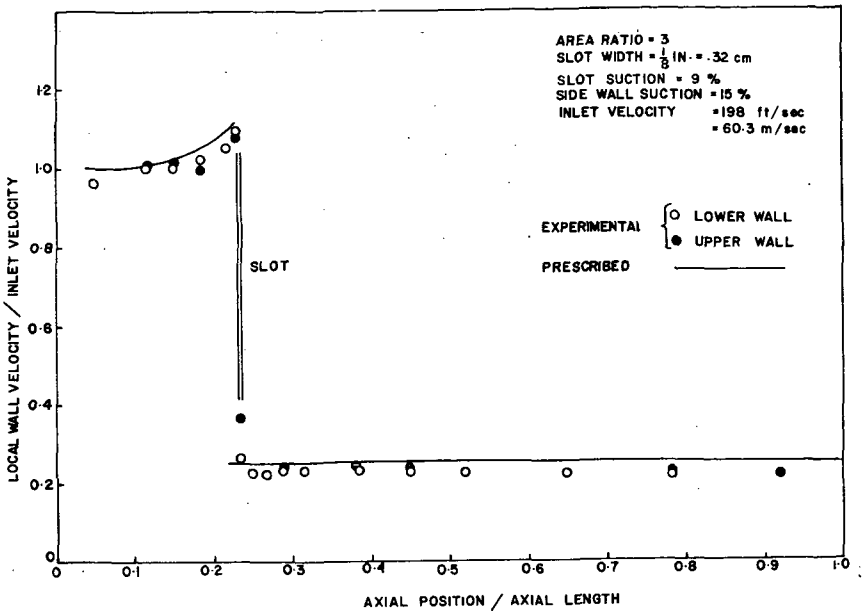

Figure 25. Wall velocity distribution for Griffith diffuser; AR = 3.

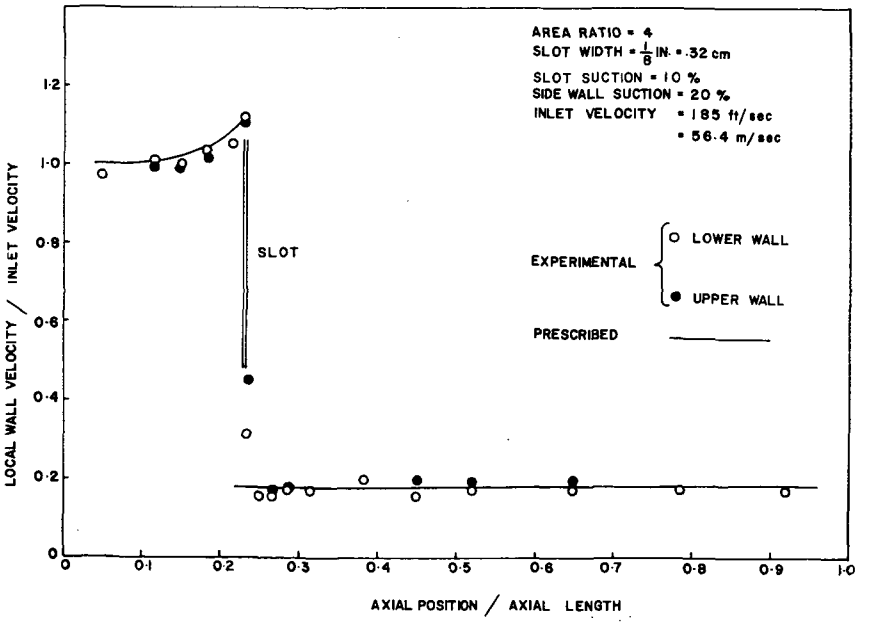

Figure 26. Wall velocity distribution for Griffith diffuser; AR = 3.

area ratios of 3 and 4 respectively. Also shown on the same figures are the wall velocity distributions prescribed to the computer design program with 5% slot suction. This would help to compare the trend rather than the values. The agreement between the measured and prescribed values of the wall velocities downstream of the suction slot is misleading. This is because of the difference in total suction between the design value and that used in the test run. For example, referring to Figure 25, the total suction used, which is the suction used for the slots and the side walls, is 24% of the inlet flow rate while the design value is only 5%. Accordingly one would expect the experimental results of the wall velocities downstream of the slot to have values lower than those prescribed to the design program. Referring again to Figure 25, the ratio of the exit velocity to inlet velocity calculated from the wall static pressure measurements is found to be 0.23. A simple flow balance yields a value of 0.25 for the same quantity which is 8% higher than the previous value (0.23). This can be attributed to the fact that the measured values of wall velocities were normalized by the inlet wall velocity which is higher than the average inlet velocity used in the flow balance calculations. A similar check is made in the case of Figure 26.

The results of the center line velocity traverses are shown in Figures 27 and 28 for the area ratios of 3 and 4 respectively. Also shown are the distributions resulting from the computer analysis program using values for slot suction equal to the total suction used in the test runs; i.e. 27% for AR = 3 (Figure 27) and 42% for AR = 4 (Figure 28). The agreement between the analysis and test results is

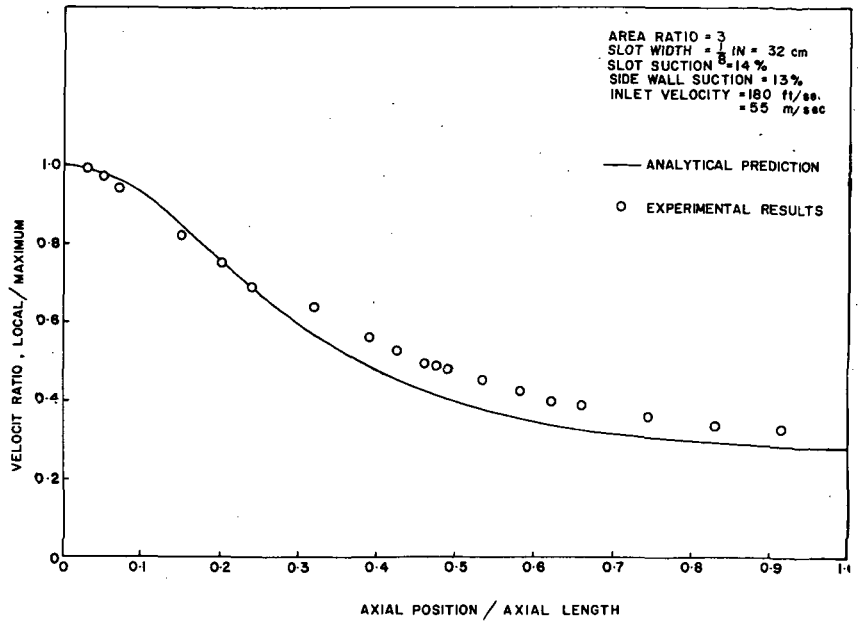

Figure 27. Center line velocity distribution for Griffith diffuser; AR = 3.

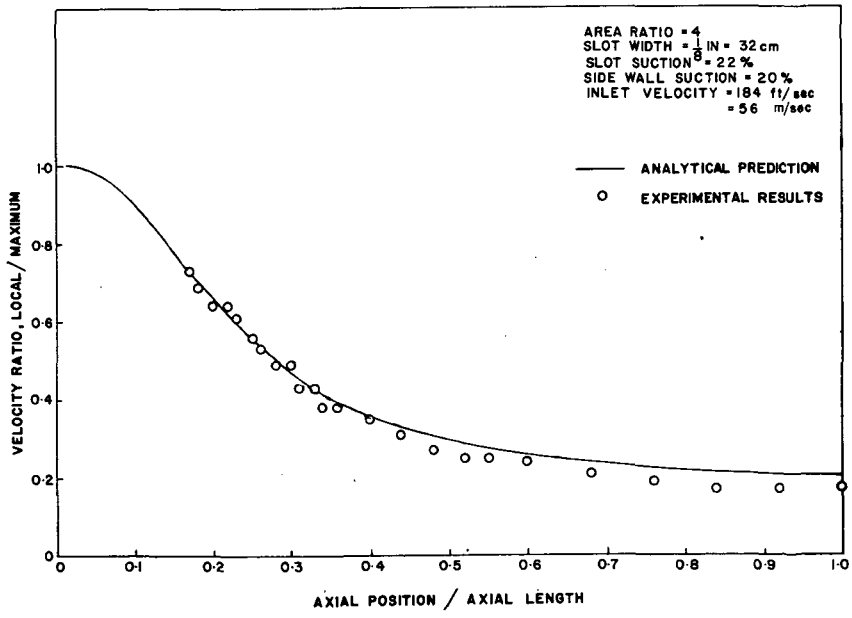

Figure 28. Center line velocity distribution for Griffith diffuser; AR = 4.

fairly good. Referring to the same figures, flow balance calculations yield the values of 0.24 and 0.14 for the ratio of the average exit to inlet velocity and for the area ratios of 3 and 4 respectively. The measured ratio for the center line velocities are slightly higher than 0.24 and 0.14 as can be seen from the same figures. This can be attributed to the fact that the center line velocity at the inlet section is lower than the average velocity at the inlet section; the velocity distribution exhibits a "dip" in the center portion.

Figures 29 and 30 show exit plane velocity maps for the diffuser with area ratios 3 and 4 when it is operating in the meta-stable condition. The inlet air velocity was kept constant at 170 ft/sec (51.8 m/sec) and the suction was adjusted to obtain a meta-stable operating condition. The contours of constant exit plant velocity exhibit a flat profile for the major portion of the exit plane. For both area ratios, a slight "dip" in exit plane velocity was observed in the area around the center while velocities near the diffuser and side walls are generally higher. Figure 31 shows the exit plane velocity distributions along the central horizontal line, C-L. The exit plane velocity distribution in the vertical direction obtained from the computer analysis program and the computer design program are shown in Figure 32, together with the measured values. The discrepancy between the theoretical and experimental results could be due to a certain degree of nonuniformity in the flow through the air duct which was transmitted to the diffuser inlet.

6.2 Dump Diffuser

It was not possible to operate the dump diffuser unseparated either in the meta-stable or stable condition using the suction capacity avail-

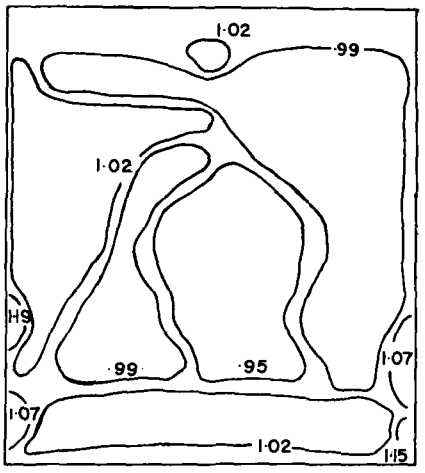

Figure 29. Exit plane velocity map for Griffith diffuser; AR = 3 (lines of constant U/U_{av})

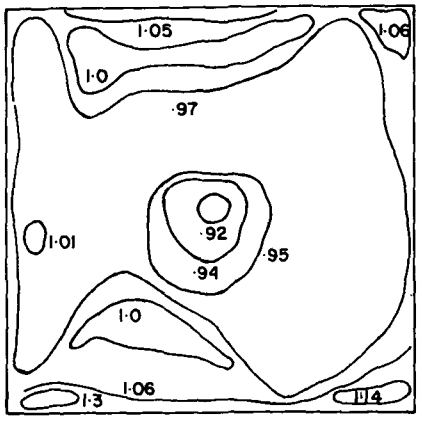

Figure 30. Exit plane velocity map for Griffith diffuser; AR = 4 (lines of constant U/U_{av})

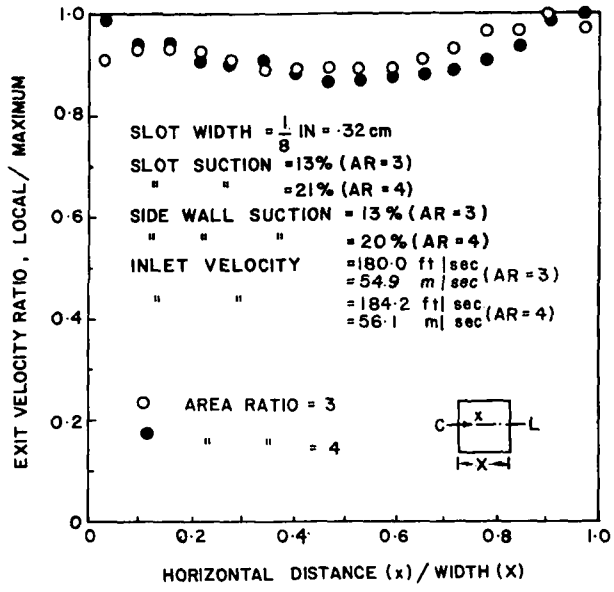

Figure 31. Exit plane velocity distribution along horizontal center line for Griffith diffuser; AR = 3 and 4.

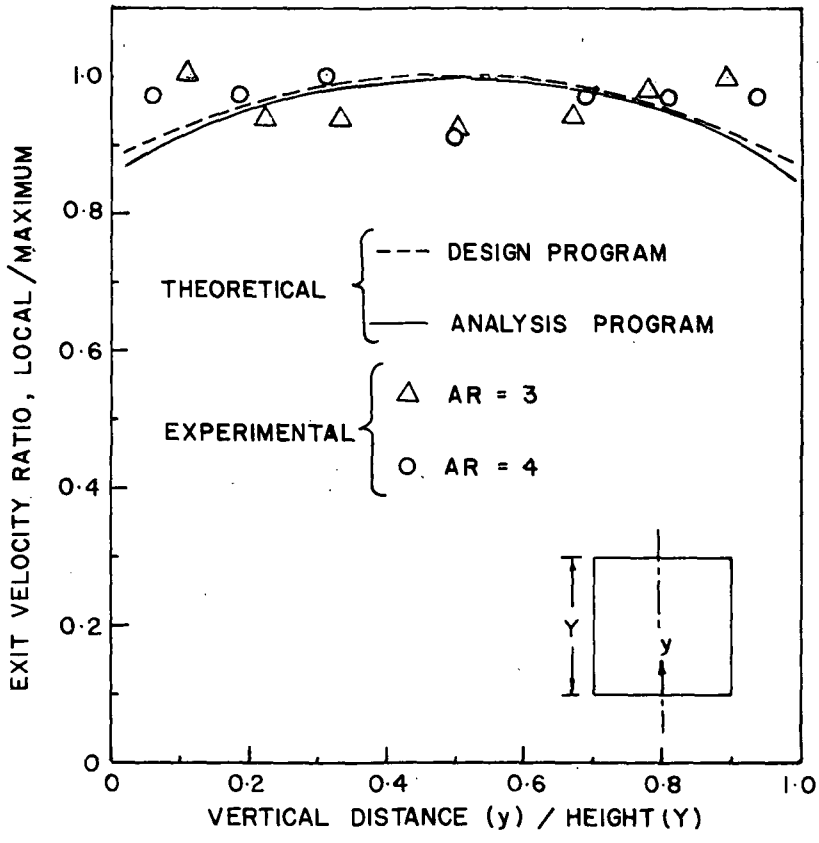

Figure 32. Exit plane velocity distribution along vertical center line for Griffith diffuser; AR = 3 and 4.

able. All measurements were taken in the separated condition. The area ratio was varied from 3 to 4 by varying the spacing between the two diffuser walls. Two suction slot locations were tested, one at the inlet corner and the other at the exit corner. The suction slots were 8 inches (20.3 cm) long and 1/16 inch (0.16 cm) wide.

Figures 33 and 34 show the values of the effectiveness obtained for the dump diffuser with an area ratio of 3 and 4 with the suction slot located at either the inlet corner or the exit corner. The slot width used for both locations was 1/16 in (0.16 cm). The slot suction and side-wall suction varied from 9% to 47% and 5% to 30% respectively. The particular values of slot and side-wall suctions for each test run are shown in Table 2. Comparing the values of the effectiveness obtained with the suction slot located at the inlet and exit corners shows that substantially higher values were obtained when the slot was located at the inlet corner.

Figures 35 and 36 show the wall velocity distribution for area ratios of 3 and 4 respectively and with the suction slots located at the inlet corners. The test conditions for both cases are: inlet velocity = 148 ft/sec (45.1 m/sec), slot suction = 33% and side-wall suction = 20%.

The exit velocity distributions are shown in Figures 37 and 38 for the area ratio of 3 and 4 respectively and for the same test conditions of Figures 35 and 36. These show a large degree of non-uniformities in comparison with the exit velocity distribution of the Griffith diffuser (see Figure 31).

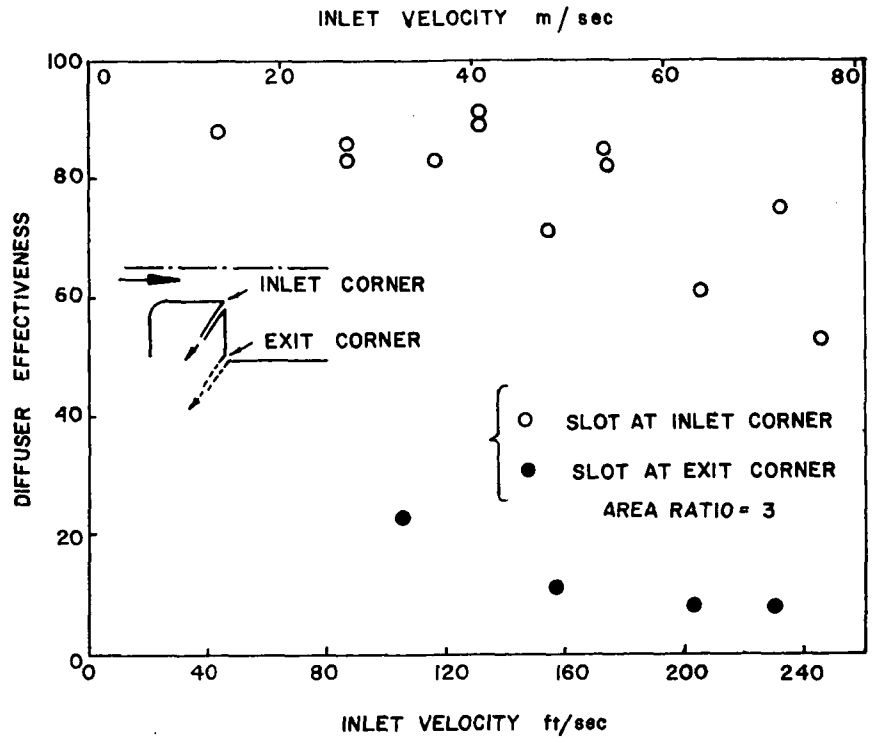

Figure 33. Effectiveness η versus inlet velocity for dump diffuser, AR = 3.

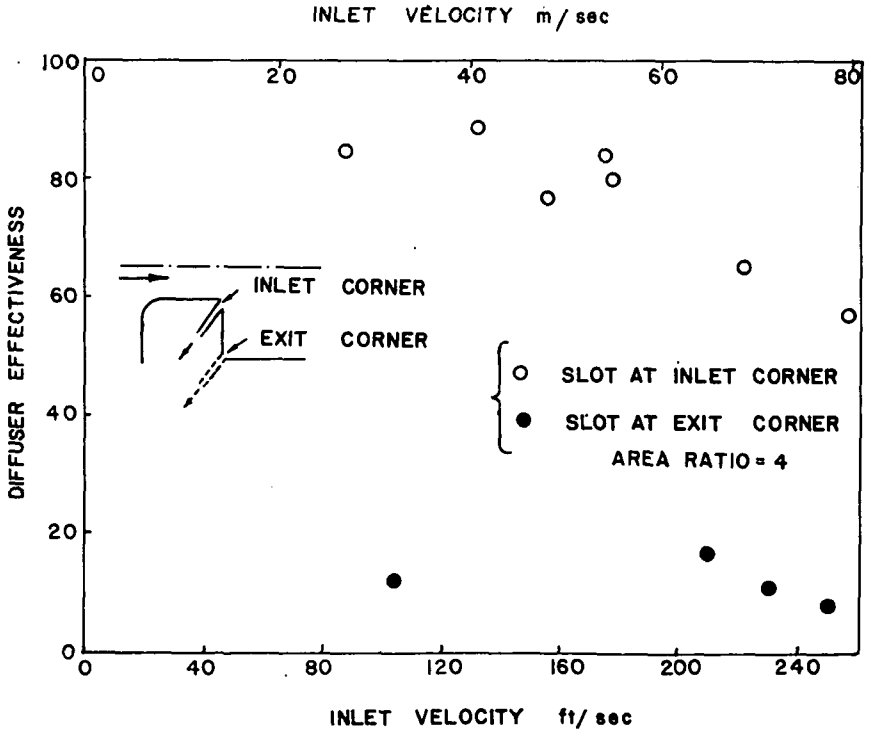

Figure 34. Effectiveness η versus inlet velocity for dump diffuser, AR = 4.

Table 2. Test Conditions and Effectiveness of Dump Diffuser

AREA RATIO, AR = 3

Slot At Inlet Corner					Slot At Exit Corner				
Inlet ft/sec	Velocity m/sec	Suction Slot	% Side Wall	Effectiveness η	Inlet ft/sec	Velocity m/sec	Suction Slot	% Side Wall	Effectiveness η
44.3	13.5	17	24	0.88	105.0	32.0	34	30	0.23
86.8	26.4	11	13	0.83	157.0	47.8	22	21	0.11
87.0	26.5	14	15	0.86	203.0	61.9	17	16	0.08
116.0	35.4	31	28	0.83	230.0	70.1	15	14	0.08
131.0	39.9	14	9	0.91					
131.0	39.9	19	12	0.89					
154.0	46.9	23	21	0.71					
173.0	52.7	14	11	0.85					
173.7	52.9	11	9	0.82					
205.0	62.5	17	16	0.61					
232.0	70.7	9	4	0.75					
232.0	70.7	11	5	0.75					

AREA RATIO, AR = 4

Slot At Inlet Corner					Slot At Exit Corner				
88.0	26.8	17	17	0.85	104.0	31.7	47	29	0.12
132.0	40.2	32	14	0.89	210.0	64.0	23	14	0.16
148.0	45.1	33	20	0.77	230.0	70.1	21	13	0.11
175.0	53.3	22	10	0.84	250.0	76.2	19	12	0.08
178.0	54.2	16	11	0.80					
222.0	67.7	22	14	0.65					
257.0	78.3	19	12	0.57					

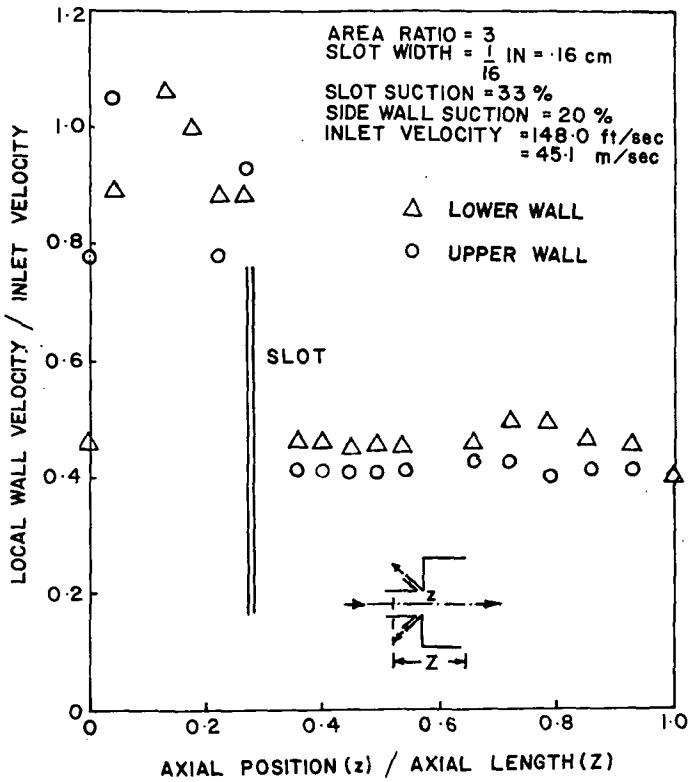

Figure 35. Wall velocity distribution for dump diffuser; AR = 4.

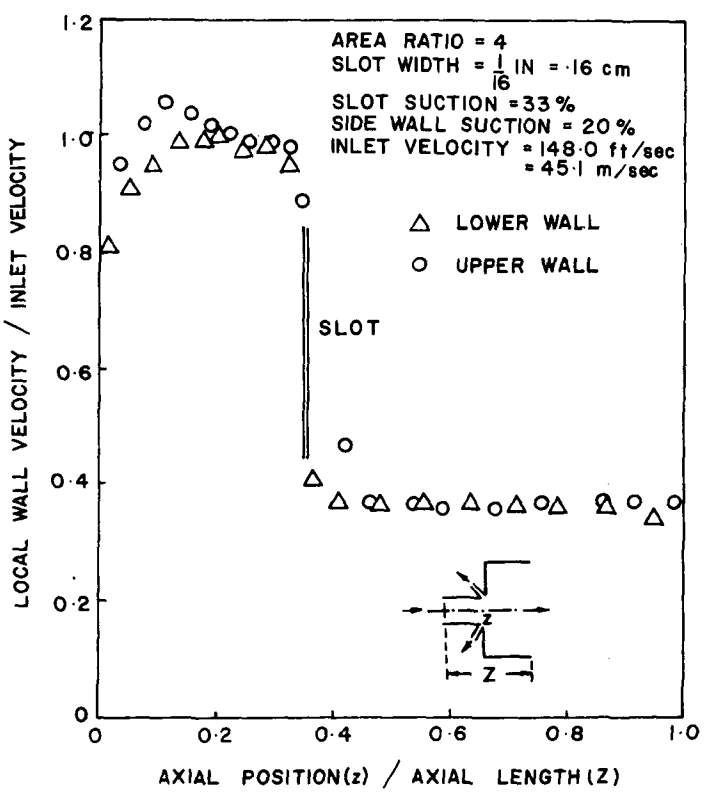

Figure 36. Wall velocity distribution for dump diffuser; AR = 4.

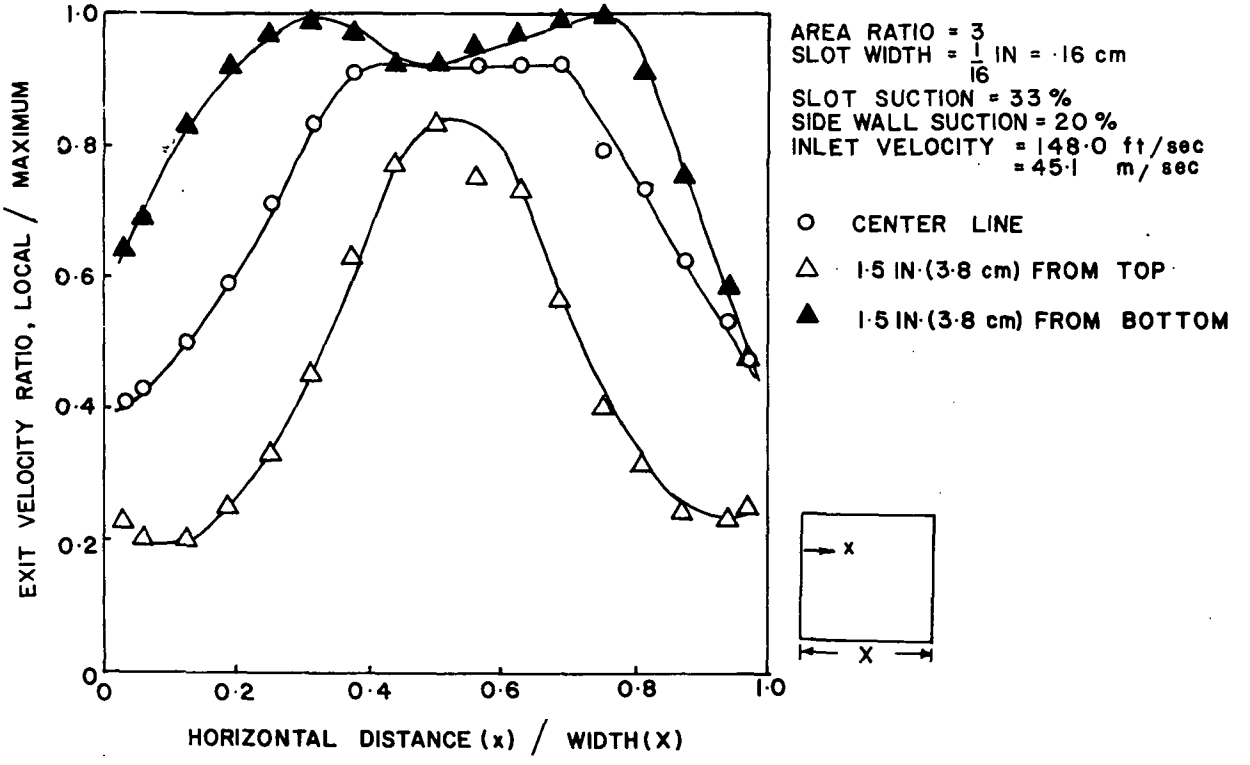

Figure 37. Exit plane velocity distribution along horizontal lines for dump diffuser; AR = 3.

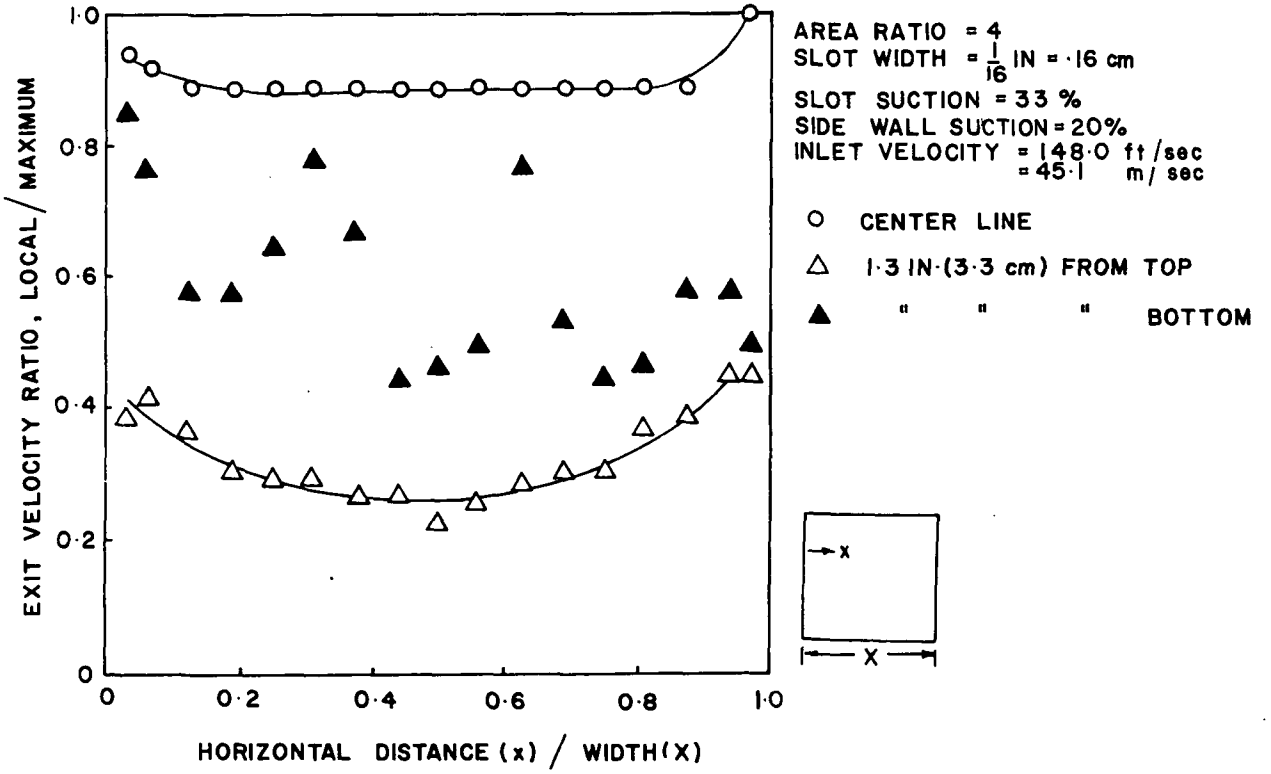

Figure 38. Exit plane velocity distribution along horizontal lines for dump diffuser; AR = 4.

6.3 Cusp Diffuser

The inlet and diffuser lengths for the cusp diffuser were chosen to be equal to the corresponding lengths for both the Griffith and the dump diffusers. The area ratios were 2.7 and 3.7, as discussed in section 4.3.

No standing vortices were observed using the available suction capacity and therefore attached flow was not possible to achieve. The flow emerged from the inlet section in the form of a jet and no pressure recovery was obtained whatsoever. The flow pattern is shown in Figure 39. In all test runs the pressure in the inlet section was higher than the pressure in the exit plane (atmospheric). Referring again to Figure 39, for an inlet velocity of U_i = 100 ft/sec (30.5 m/s), typical values of the static pressure at several locations were as follows:

$P_o - P_i$ = 2.6 inch H_2O (6.6 cm H_2O)

$P_i - P_c$ = 1.2 inch H_2O (3.0 cm H_2O)

$P_c - P_t$ = 1.0 inch H_2O (2.54 cm H_2O)

$P_t - P_{atm}$ = 0.0 inch H_2O (0.0 cm H_2O)

P_c is the stream pressure at the cusp location, P_t is the pressure at the vena contracta, P_i is the pressure at the inlet section and P_o is the stagnation pressure. These figures show that no pressure recovery was achieved and the channel did not act as a diffuser. It is believed that a longer diffuser length is needed to achieve unseparated flow with two standing vortices than the length which was used (6.2 in (15.7 cm)).

An exit velocity map is shown in Figure 40 which shows regions of backflow near the diffuser walls.

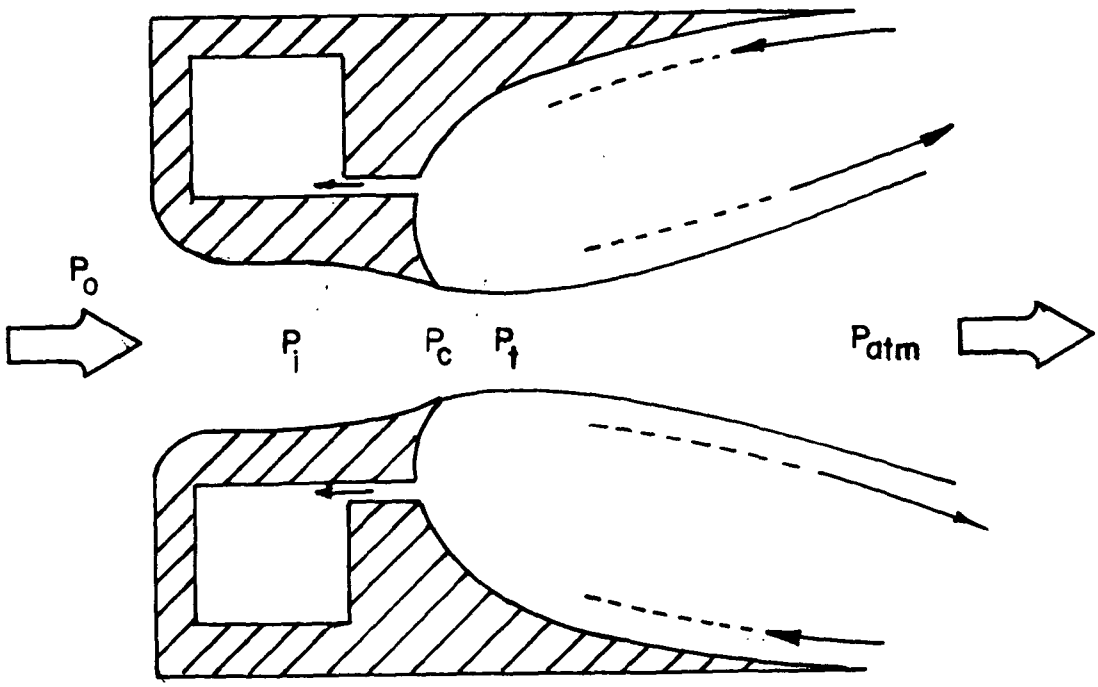

Figure 39. Flow pattern in cusp diffuser, AR = 2.7.

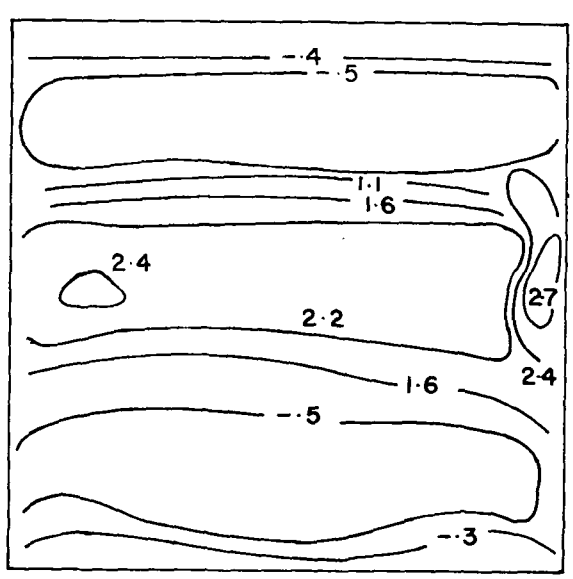

AREA RATIO = 2.7
SLOT WIDTH = $\frac{1}{16}$ IN = .16 cm
SLOT SUCTION = 18 %
SIDE WALL SUCTION = 4 %
INLET VELOCITY = 170.6 ft/sec
= 52.0 m/sec

Figure 40. Exit plane velocity map for cusp diffuser; AR = 2.7 (lines of constant U/U_{av}).

SECTION VII

CONCLUSIONS

7.1 Griffith Diffuser

In a metastable operating condition, slot suction rates around 8% of the inlet through flow rate was required to prevent flow separation for AR = 4, provided that adequate side-wall suction was applied. For AR = 3, the values of slot suction rates were about 25% lower than those required for the higher area ratio. For stable operation, slot suction rates of approximately 30% were required with the diffuser of AR = 4, and 28% with the diffuser of AR = 3. For nearly all the unseparated test runs, the diffuser effectiveness η was 100%.

7.2 Dump Diffuser

The location of the suction slot proved to be critical as regards the diffuser effectiveness η. Much higher values of diffuser effectiveness were observed with the slot located at the inlet corner in contrast to the exit corner. However, flow separation occurred in all test runs.

7.3 Cusp Diffuser

Using the same inlet and diffuser lengths as for the Griffith and dump diffusers, 1 in (2.54) cm for inlet and 6.2 in (15.7) cm for diffuser lengths, it was not possible to achieve unseparated flow with two standing vortices in the cusp diffuser. The flow behaved as a jet emerging from the inlet section and no pressure recovery was obtained. It is believed that unseparated flow with two standing vortices could be achieved using a diffuser length longer than the one used in this investigation.

SECTION VIII

REFERENCES

1. Yang, T.T. and Hudson, W.G.: "Proposed Design and Experimental Performance of Short Two Dimensional Curved Wall Diffusers Utilizing Suction Slots", NASA CR-120783, September 1971.

2. Griffith, A.A.: "Reducing Surface Friction Between a Solid and a Fluid", Patent 578, 763 (Great Britain), August 1942.

3. Ringleb, F.O.: "Two Dimensional Flow with Standing Vortexes in Ducts and Diffusers", Transaction of the ASME, Journal of Basic Engineering, pages 921-928, Series D, Vol. 82, 1960.

4. Perkins, C.D. and Hazen, D.C.: "Some Recent Advances in Boundary Layer and Circulation Control", Fourth Anglo-American Aeronautical Conference, London, England, 1953.

5. Nelson, C.D., Jr.: "An Analytical Design Method and Experimental Results for Axially Symmetrical Diffusers Having Incompressible, Unseparated Flow and Employing Slot Suction", Ph.D. Dissertation, Clemson University, August 1971.

6. Hess, J.L. and Smith, A.M.O.: "Calculation of Potential Flow about Arbitrary Bodies", Progress in Aeronautical Sciences, Vol. 8, D. Kuchemann, ed., Pergamon Press, 1967, pages 1-138.

7. Goldstein, S.: "Low Drag and Suction Airfoils", Journal of Aeronautical Sciences, Vol. 15, No. 4, April 1948.

8. Stanitz, J.D.: "Design of Two Dimensional Channels with Prescribed Velocity Distributions along the Channel Walls", NACA Report 1115, 1953.

9. Schlichting, H.: "Boundary Layer Theory", McGraw-Hill, 1968.

APPENDIX A

Outline of Surface - Source - Distribution Method In Solving Channel Flow Problems Using Cascade Theory

In determining the flow field around non-lifting bodies, the surface - source - distribution method is used. The basic idea is to cover the body surface with a continuous distribution of sources (or sinks) and to adjust the strength of this distribution so that the total velocity normal to the body surface is either zero (impermeable wall) or a prescribed value (permeable wall). Once the distribution of sources is known, the flow field is completely determined. The aim now is to outline the method by which this distribution could be obtained.

Consider the flow around a two-dimensional body as shown in Figure 41. U_∞ is the velocity vector which represents the stream velocity upstream of the body. Let U_n represent the prescribed velocity normal to the

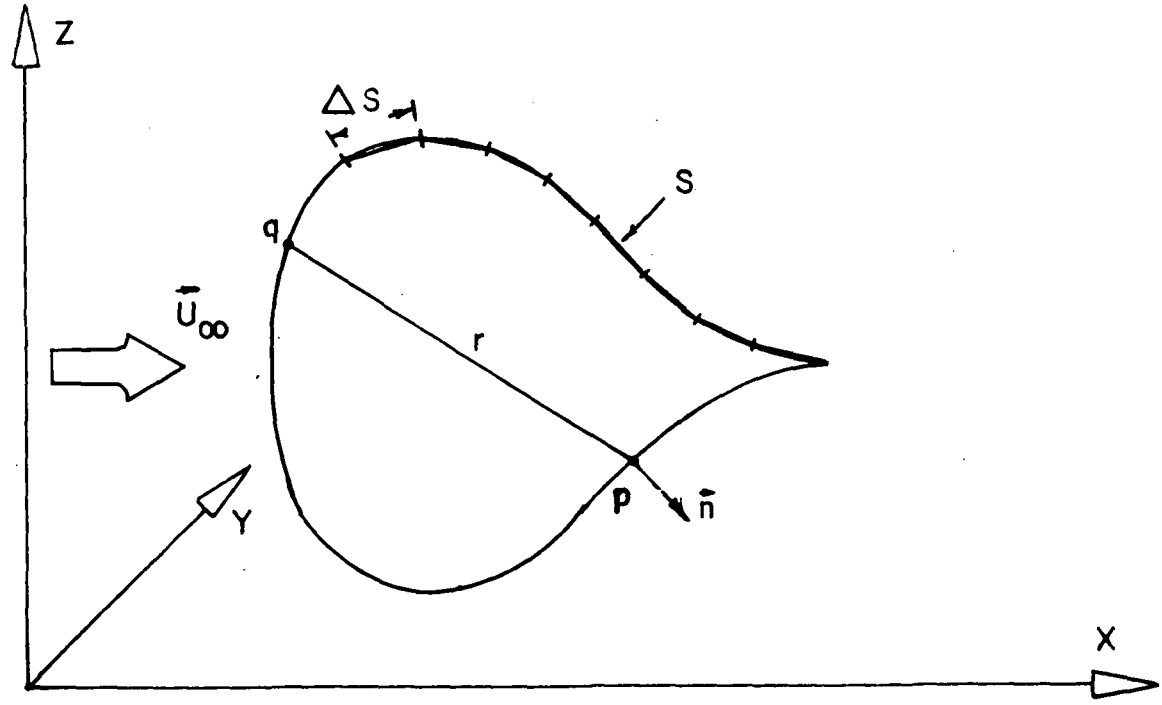

Figure 41. Geometry of two dimensional body

surface, for a solid surface $U_n = 0$. If ϕ is the potential due to the source distribution at a particular point p on the surface, then the velocity normal to the surface at point p must be made up of two parts according to the equation

$$U_n = \vec{U}_\infty \cdot \vec{n} + \frac{\partial \phi}{\partial n} \qquad 32$$

where $\vec{n}$ is the outward normal vector

In this equation $\vec{U}_\infty \cdot \vec{n}$ represents the component of $\vec{U}_\infty$ normal to the surface at point p. The term $\frac{\partial \phi}{\partial n}$ represents the contribution of the potential due to the yet unknown source distribution, henceforth, called disturbance potential. If the source - distribution per unit area at any point q is denoted by $\sigma(q)$, then the potential at p due to a source $\sigma(q)\sigma S$ at q is given by the equation:

$$\delta\phi(p) = \sigma(q) \frac{1}{r} \delta S$$

The distrubance potential at p due to the total source distribution over the entire body surface S is given by:

$$\phi(p) = \iint_S \sigma(q) \frac{1}{r} dS \qquad 33$$

The point p need not be on the surface, as shown in Figure 41, since equation 33 is equally applicable if p is off the body surface. The fluid velocities in the three directions of a Cartesian coordinate system x, y, and z, are $\partial\phi(p)/\partial x$, $\partial\phi(p)/\partial z$ respectively. The velocity vector at point p is given by:

$$\vec{U} = \frac{\partial \phi(p)}{\partial x} \vec{i} + \frac{\partial \phi(p)}{\partial y} \vec{j} + \frac{\partial \phi(p)}{\partial z} \vec{k} \equiv \text{grad } \phi(p) \qquad 34$$

where $\vec{i}$, $\vec{j}$, and $\vec{k}$ are the unit vectors along the x, y, and z coordinates respectively.

From equations 33 and 34 , equation 35 can be derived:

$$\text{grad } \phi(p) = \iint_S \sigma(q) \text{ grad } \left(\frac{1}{r}\right) dS \qquad 35$$

Using equation 35 the boundary condition expressed in equation 32 can be written as:

$$U_n - (\vec{U}_\infty \cdot \vec{n}) = \iint_S \sigma(q) \frac{\partial}{\partial n} \left(\frac{1}{r}\right) dS \qquad 36$$

For a known body contour and a known free stream velocity $\vec{U}_\infty$, equation 36 can be solved using numerical integration to yield the source distribution $\sigma(q)$. Once the source distribution $\sigma(q)$ is known, the flow field is determined.

In solving equation 36 numerically, the body contour is approximated by line segments and assuming that the source density $\sigma(q)$ is constant along each segment, see Figure 41 . Letting the number of segments be N, and using summation instead of integration, equation 36 can now be written as:

$$U_n - (\vec{U}_\infty \cdot \vec{n}) = \sum_{q=1}^{N} A_{pq} \sigma(q) \qquad 37$$

where $A_{pq} = \frac{\partial}{\partial n} \left(\frac{1}{r}\right) \Delta S$ and ΔS is the area of the element considered. Equation 36 represents one equation in N unknown source strengths, $\sigma(q)$, where q varies from 1 to N. To obtain N equations, the point p is allowed to change position from element 1 to N. Hence, we obtain a set of N simultaneous equations in N unknowns. An expression analogous to that of 36 can be written for the tangential components due to the disturbance potential, $\frac{\partial \phi(p)}{\partial t}$. Thus,

$$\frac{\partial \phi(p)}{\partial t} = \sum_{q=1}^{N} B_{pq} \sigma(q) \qquad 38$$

In equations 37 and 38. A_{pq} and B_{pq} are respectively, the normal and tangential velocities, at point p due to a unit source strength at point q. The total velocity due to the disturbance potential is the resultant of the normal and tangential velocities, and is given by equation 39

$$\text{grad } \phi(p) = \sum_{q=1}^{N} (A_{pq}\vec{i} + B_{pq}\vec{j})\ \sigma(q) \qquad 39$$

In order to evaluate the coefficients A_{pq} and B_{pq} at point p due to the influence of a source distribution of unit strength along the segment at q, the concept of complex velocity is used for convenience. For two-dimensional flow, the complex velocity at point p, W_{pq}, is given by:

$$W_{pq} = U_x - i\ U_y \qquad 40$$

where U_x and U_y are the velocity components along the x and y axes respectively.

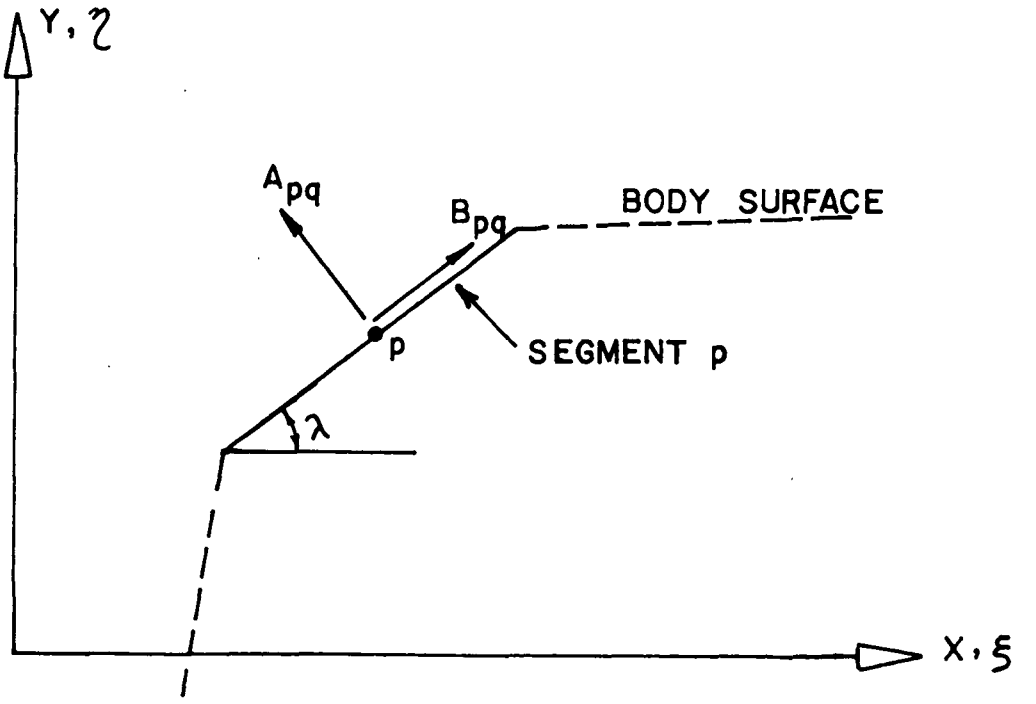

Figure 42. Normal and tangential velocities at p

Figure 42 shows an enlarged sketch of the segment at point p, the rest of the body surface is shown dotted. The normal and tangential velocities at p due to a unit source distribution along the segment at q are shown; A_{pq} and B_{pq} respectively. The segment at p is shown to be inclined at an angle of λ to the x-axis. From Figure 42 it can be shown that:

$$\left.\begin{aligned} U_x &= B_{pq} \cos\lambda - A_{pq} \sin\lambda \\ \text{and} \\ U_y &= B_{pq} \sin\lambda + A_{pq} \cos\lambda \end{aligned}\right\} \qquad 41$$

It is obvious from equations 40 and 41 that once the complex velocity is known, the coefficients A_{pq} and B_{pq} can be determined using equation 40

To evaluate W_{pq}, consider the complex velocity at point p due to a source distribution of unit strength per unit length along the segment q. Figure 43 shows an enlarged sketch of the segment q with point p

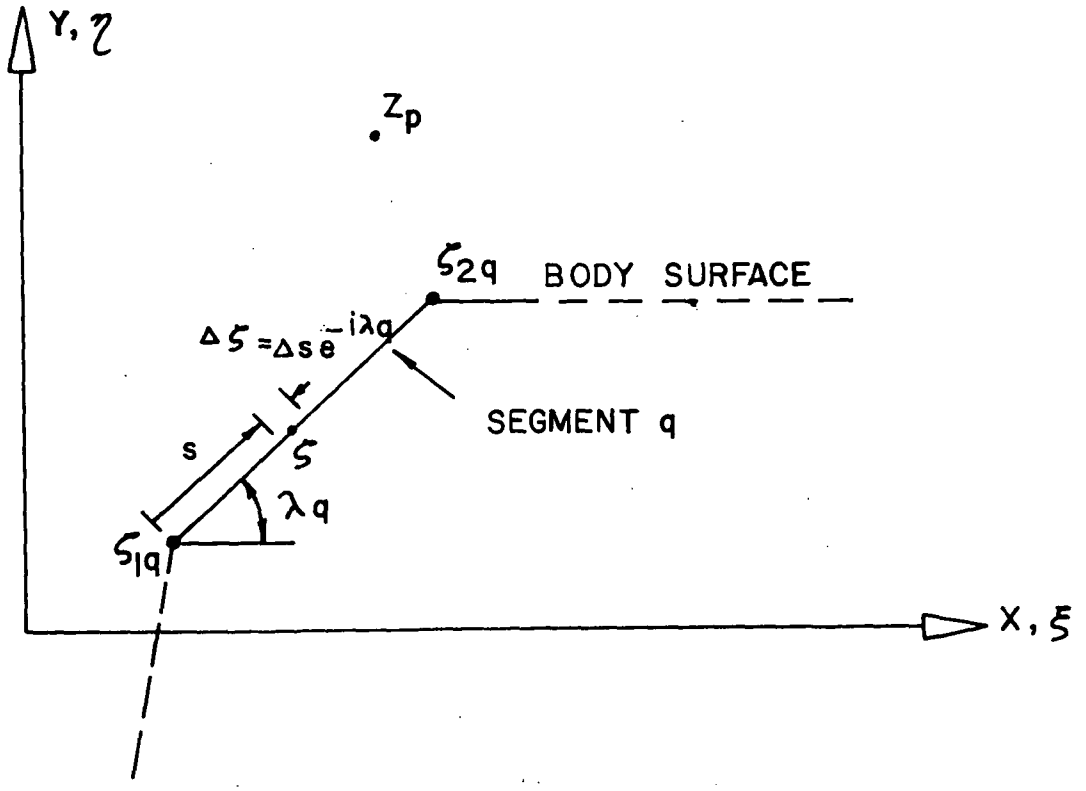

Figure 43. Segment q with point p outside body surface

drawn outside the body surface. Let Z_p be the complex coordinates of point p; $Z_p = x_p + iY_p$; and ζ_q be the complex coordinates of point q; $\zeta_q = \xi_q + i\eta_q$. It can be shown that the complex potential F (defined as $\phi + i\psi$) at point p due to a unit source located at $\zeta(s)$ is given by:

$$F = \frac{1}{2\pi} \ln [Z_p - \zeta(s)] \qquad 42$$

The complex velocity at point p is given by

$$\frac{dF}{dZ} = \frac{1}{2\pi} \frac{d}{dZ} \ln [Z_p - \zeta(s)] \qquad 43$$

The complex velocity at point p due to the segment q having a unit source strength distribution per unit length. This can be derived by integrating equation 43 along the length of the segment q from ζ_{1q} to ζ_{2q}, see Figure

$$W_{pq} = \frac{1}{2\pi} \int_{\text{segment q}} \frac{d}{dZ} \ln [Z_p - \zeta(s)] \, ds \qquad 44$$

where ds is an infinitesimal length along the segment. The same Figure also illustrates the following relationship:

$$ds \, e^{-i\lambda q} = d\zeta \qquad 45$$

Replacing ds from equation 45 into equation 44 gives:

$$W_{pq} = \frac{e^{-i\lambda q}}{2\pi} \int_{\zeta_{1q}}^{\zeta_{2q}} \frac{d}{dZ_p} \ln (Z_p - \zeta) \, d\zeta$$

$$= \frac{e^{-i\lambda q}}{2\pi} \ln (Z_p - \zeta) \Big|_{\zeta_{1q}}^{\zeta_{2q}}$$

$$= \frac{e^{-i\lambda q}}{2\pi} \ln \frac{(Z_p - \zeta_{1q})}{(Z_p - \zeta_{2q})} \qquad 46$$

The flow channel of the two-dimensional diffuser may be analyzed as a cascade problem, see Figure 44 . The flow and the body - surface - source

density is identical for each body. Equation 46 is no longer valid for the cascade problem. It can be shown that the new expression for W_{pq} is given by equation 47.

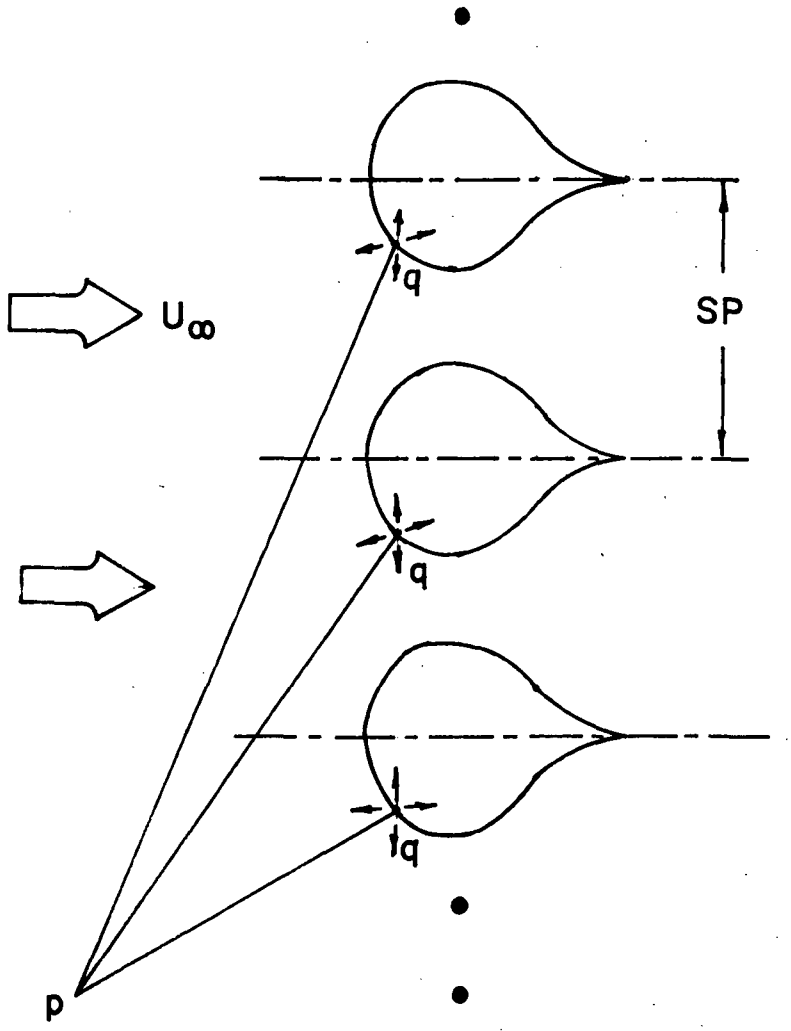

Figure 44. Flow channel represented by a cascade of bodies

$$W_{pq} = \frac{e^{-i\lambda q}}{2} \ln \left[\frac{\text{sink } [(\pi/SP)(Z_p - \zeta_{1q})]}{\text{sink } [(\pi/SP)(Z_p - \zeta_{2q})]} \right] \qquad 47$$

The numerical computations were performed using a digital computer to solve N simultaneous equations similar to equation 36 which result in obtaining the source distribution $\sigma(q)$ and hence the flow field.

APPENDIX B

Derivation Of The Expression For The Diffuser Effectiveness

The basic definition of the diffuser effectiveness is defined as the ratio between the actual and the ideal pressure recovery.

$$\eta = \frac{P_e - P_i}{(P_e - P_i)_{ideal}} \tag{48}$$

The ideal pressure recovery is derived from Bernoulli's equation as follows:

$$(P_e - P_i)_{ideal} = \frac{\rho}{2} (U_i^2 - U_e^2) \tag{49}$$

With no suction, U_e will be:

$$U_e = \frac{1}{AR} U_i$$

With suction, U_e will be:

$$U_e = \frac{\left(1 - \frac{\% \text{ suction}}{100}\right)}{AR} U_i \tag{50}$$

Substituting this value of U_e into equation 49 we get:

$$(P_e - P_i)_{ideal} = (P_o - P_i) \left[1 - \left(\frac{1 - \frac{\% \text{ suction}}{100}}{AR}\right)^2\right] \tag{51}$$

where $(P_o - P_i)$ was substituted for $\frac{1}{2} \rho U_i^2$ in equation 51. Substituting this value of $(P_e - P_i)_{ideal}$ into equation 48, the final expression for the diffuser effectiveness is obtained

$$\eta = \frac{P_e - P_i}{(P_o - P_i) \left[1 - \left(\frac{1 - \frac{\% \text{ suction}}{100}}{AR}\right)^2\right]} \tag{52}$$

FINAL REPORT DISTRIBUTION LIST FOR NASA CR-121024, Grant 41-001-031

1. NASA - Lewis Research Center
   21000 Brookpark Road
   Cleveland, Ohio 44135
   Attention:

Report Control Office	MS	5-5	1
Technology Utilization		3-19	1
Library		60-3	2
Fluid Systems Components Division		5-3	1
W.L. Stewart		77-2	1
L. Schopen		500-206	1
J.B. Esgar		60-4	1
W.T. Olson		3-16	1
R.A. Rudey		60-6	1
J.F. Dugan, Jr.		86-1	1
Seymour Lieblein		501-5	1
R.E. Jones		60-6	1
Jack Grobman		60-6	1
Lt. Col. G.S. Weden		500-317	1
James A. Albers		501-2	1
A.J. Juhasz		60-4	10

2. Mr. L. Magitti
   Naval Air Propulsion Test Center
   Bldg. 600
   Philadelphia Naval Base
   Philadelphia, Pennsylvania 19112 — 1

3. Aerospace Research Laboratory
   Wright-Patterson AFB, Ohio 45433
   Attention: Dr. R.G. Dunn — 1

4. NASA Scientific and Technical Information Facility
   P.O. Box 33
   College Park, Maryland 20740
   Attention: NASA Representative
   RQT-2448 — 6

5. FAA Headquarters
   800 Independence Avenue, S.W.
   Washington, D.C. 20533
   Attention: William Westfield — 1
   Library — 1

6. NASA Headquarters
600 Independence Avenue, S.W.
Washington, D.C. 20546
Attention: N.F. Rekos (RAP) 1
W.H. Roudebush (RAA) 1

7. Department of the Army
U.S. Army Aviation Material Laboratory
Propulsion Division (SAUFE-PP)
Fort Eustis, Virginia 23604
Attention: J. White 1
E.T. Johnson 1

8. United Aircraft of Canada, Ltd.
P.O. Box
Lonquenil, Quebec, Canada
Attention: Miss Mary Cullen 1

9. Air Force Office of Scientific Research
1400 Wilson Boulevard
Arlington, Virginia 22209
Attention: SREP 1

10. Defense Documentation Center (DDC)
Cameron Station
5010 Duke Street
Alexandria, Virginia 22314 1

11. Department of the Navy
Bureau of Naval Weapons
Washington, D.C. 20025
Attention: Robert Brown, RAPP14 1

12. Department of the Navy
Bureau of Ships
Washington, D.C. 20360
Attention: G.L. Graves 1

13. NASA-Langley Research Center
Langley Station
Technical Library
Hampton, Virginia 23365
Attention: Mark R. Nichols 1
John V. Becker 1
Richard J. Margajon MS 404 1

14. United States Air Force
    Aero Propulsion Laboratory
    Area B, Bldg. 18D
    Wright-Patterson A.F.B.
    Dayton, Ohio 45433
    Attention: Robert E. Henderson — 1

15. United Aircraft Corporation
    Pratt & Whitney Aircraft Division
    400 Main Street
    East Hartford, Connecticut 06108
    Attention: G. Andreini — 1
    Library — 1
    R. Marshall — 1

16. United Aircraft Research
    East Hartford, Connecticut
    Attention: Library — 1

17. Detroit Diesel Allison Division
    Department 8894, Plant 8
    P.O. Box 894
    Indianapolis, Indiana 46206
    Attention: J.N. Barney — 1
    G.E. Holbrook — 1
    Library — 1

18. Northern Research & Engineering Corp.
    219 Vassar Street
    Cambridge, Massachusetts 02139
    Attention: K. Ginwala — 1

19. General Electric Company
    Flight Propulsion Division
    Cincinnati, Ohio 45215 — 1
    Attention: J.S. McBridge H-44 — 1
    F. Burggraf H-32 — 1
    C. Danforth H-32 — 1
    Technical Information Center N-32 — 1
    D. Bahr — 1

20. General Electric Company
    1000 Western Avenue
    West Lynn, Massachusetts 01905
    Attention: Dr. C.W. Smith
    Library Building 2-40M — 1

21. Curtiss-Wright Corporation
Wright Aeronautical Division
Wood-Ridge, New Jersey 07075
Attention: D. Wagner 1
W. Walker 1

22. Air Research Manufacturing Company
402 South 36th Street
Phoenix, Arizona 85034
Attention: Robert O. Bullock 1

23. Air Research Manufacturing Company
9851 Sepulveda Boulevard
Los Angeles, California 90009
Attention: Mr. L.C. Wright 1

24. AVCO Corporation
Lycoming Division
550 South Main Street
Stratford, Connecticut
Attention: Claus W. Bolton 1
Charles Kuintzle 1

25. Continental Aviation & Engineering Corporation
12700 Kercheval
Detroit, Michigan 48215
Attention: Eli H. Bernstein 1
Howard C. Walch 1

26. International Harvester Company
Solar Divison
2200 Pacific Highway
San Diego, California 92112
Attention: P.A. Pitt 1

27. Goodyear Atomic Corporation
Box 628
Piketon, Ohio
Attention: C.O. Langebrake 1

28. George Derderian AIR 53622 B
Department of the Navy
Bureau of the Navy
Washington, D.C. 20360 1

29. The Boeing Company
Commercial Airplane Division
P.O. Box 3991
Seattle, Washington 98124
Attention: G.J. Schott MS 80-66 1

30. The Boeing Company
Missile and Information Systems Division
224 N. Wilkinson Street
Dayton, Ohio 45402
Attention: Warren K. Thorson 1

31. Aerojet-General Corporation
Sacramento, California 95809
Attention: M.S. Nylin 1
Library 1

32. Cornell Aeronautical Laboratory
4455 Genessee Street
Buffalo, New York 14221 1

33. Marquardt Corporation
16555 Saticoy Street
Van Nuys, California 1

34. Thompson Ramo Wooldridge
23555 Euclid Avenue
Cleveland, Ohio 1

35. Aro, Incorporated
Arnold Air Force Station
Tennessee 1

36. The Johns Hopkins University
Applied Physics Laboratory
Silver Spring, Maryland 20910
8621 Georgia Ave.
Attn: W.B. Shippen 1
Dr. G. Dugger 1

37. Cummings Engine Co.
Cummings Technical Center
1900 McKinley Avenue
Columbus, Indiana 47201
Attention: Curt Dasbach
Mail Code 50142 1

38. Garrett/AiResearch Co.
402 South 36th Street
Phoenix, Arizona 85034
Attention: John M. Haasis 1

39. Pratt & Whitney Aircraft
Florida Research & Development Center
Box 2691
West Palm Beach, Florida 33402
Attention: J. Chamberlain 1
J. Dykslag 1
J. Shadowen 1
G. Lewis 1

40. Professor A.H. Lefebre
The Cranfield Institute of Technology
Cranfield, Bedford
Great Britain 1

41. Aerojet General Corporation
Sacramento Facility
P.O. Box 15847
Sacramento, California 95813
Attention: C.E. Tedmon 1
Dave Kors 1

42. The University of Toledo
Toledo, Ohio 43606
Attention: Dr. Duen-Ten Jeng 1
Dr. Kenneth DeWitt 1

43. Eaton Yale and Towne Research Center
26201 Northwestern Highway
Southfield, Michigan 48075 1

44. Rocketdyne
North American Rockwell
6630 Canoga Avenue
Canoga Park, California 91304
Attention: S.D. Clapp
Manager
Propulsion Technology Research Division 1

45. Dept. of Mechanical Engineering
201 Engineering Building
Michigan State University
E. Lansing, Michigan 48823
Attention: Dr. Merle C. Potter 2

46. Department of Engineering
Leicester University
Leicester, Great Britain
Attention: Dr. David J. Cockrell 1

47. Von Karman Institute for Fluid Dynamics
Chaussee de Waterloo 72
1640 Rhode-St-Gense (Beligique)
Attention: Professor J. Chaurvin 1

48. Simon Laboratories
University of Manchester
Manchester, Great Britain
Attention: Dr. John Turner 1

49. Engineering Department
Salford University
Manchester, Great Britain
Attention: Dr. Wilcox 1

50. Engineering Department
University of Liverpool
Liverpool, Great Britain
Attention: Professor J.C. Gibbings

51. Gas Turbine Department
General Electric Co.
Schenectady, New York
Attention: R.L. Hendrickson 1

52. School of Mechanical and Aerospace Engineering
Upson Hall
Cornell University
Ithaca, New York
Attention: Professor E.R. Resler 1
Professor D.G. Shaphard 1

53. School of Engineering
University of Auckland
Privatebag, Auckland
New Zealand
Attention: Dr. G.L. Bowen 1

54. Technical Center
Cummings Engineering Co.
Columbus, Indiana
Attention: Dr. A.C. Chu 1

55. Mechanical Engineering Department
Iowa State University
Ames, Iowa 50010
Attention: Professor George K. Serovy 1

56. Mechanical and Aerospace Engineering Dept.
University of Tennessee
Knoxville, Tennessee
Attention: Professor Mancil Milligan 1

57. Department of Mechanical Engineering
Virginia Polytechnic Inst. & State Univ.
Blacksburg, Virginia 24061
Attention: Professor Felix J. Pierce 1

58. Department of Mechanical Engineering
Purdue University
Lafayette, Indiana
Attention: Dr. A.T. McDonald 1

59. McDonald-Douglas Aircraft Co.
St. Louis, Missouri 63166
Attention: Dr. E.D. Spong 1
Dept. 243

60. Aerospace Group System Division
Hughes Aircraft Co.
Canoga Park, California 91304
Attention: Mr. J.L. Raymond 1

61. Lehigh University
Bethlehan, Pennsylvania 18015
Attention: Dr. Donald O. Rockwell 1